

## Electronic Supplementary Information

for

### **pH Triggered superior selective adsorption and separation of both the cationic and anionic dyes and photocatalytic activity on fully exfoliated titanate layer –natural polymer based nanocomposite**

Amit Kumar Sarkar,<sup>a</sup> Arka Saha,<sup>b</sup> Asit Baran Panda,<sup>\*b</sup> Sagar Pal<sup>\*a</sup>

*<sup>a</sup> Polymer Chemistry Laboratory, Department of Applied Chemistry, Indian School of Mines, Dhanbad-826004, India*

*Tel: 91-326-2235769; Fax: 91-326-2296615, E-mail: sagarpall@hotmail.com*

*<sup>b</sup> Discipline of Inorganic Materials and Catalysis, Central salt and Marine Chemicals Research Institute (CSIR), Bhavnagar-364002, Gujarat, India*

*E-mail: abpanda@csmcri.org, web: <http://abpandasgroup.webs.com>*

# **Contents:**

## **S1. Experimental sections**

Synthesis

Characterizations

Adsorption, desorption and photodegradation experiments

## **S2. Results and discussions**

Nanocomposite characterization

Adsorption optimizations

Adsorption Kinetics

Adsorption isotherm

Adsorption thermodynamics

Regeneration Study

- Desorption study

- Photodegradation study

## **S1. EXPERIMENTAL SECTION**

### **MATERIALS:**

Amylopectin (source: maize) was procured from Fluka, Switzerland. Titanium isopropoxide and 2-(diethyl amino ethyl) methacrylate (DEAEMA) were purchased from Sigma Aldrich, USA. DEAEMA was distilled using  $\text{CaH}_2$  under reduced pressure. Methanol, acetone, ammonia, ammonium chloride, sodium hydroxide (E. Merck, Mumbai, India), methylene blue (MB), methyl orange (MO), malachite green (MG) (Loba Chemie Pvt. Ltd., Mumbai, India), RB (received as gift sample from Hindustan Gum & Chemicals Ltd., Bhiwani, Haryana) were of analytical grade and used as received. Potassium persulfate was procured from Qualigens, Mumbai, India. In all experimental work, milli Q water was used.

### **SYNTHESIS:**

#### ***Preparation of AP-g-p (DEAEMA):***

The cationic *graft* copolymer was synthesized using free radical polymerization technique.<sup>1</sup> The polymerization was carried out in nitrogen atmosphere using three necked round-bottom flask. The RB flask was integrally joined with an electrically operated magnetic stirrer (Tarsons, Model: Spinot Digital) to dissolve the reactants. The whole system was kept in an oil bath with a temperature controller to obtain a desired temperature. 1 g of amylopectin was slowly dissolved into 60 mL of distilled water in a RB flask. Then temperature was maintained at 80° C with constant stirring (400 rpm). Afterwards, potassium persulphate of required concentration (Table S1) was added under nitrogen bubbling for 15 min. The same temperature was maintained

throughout the reaction period. After 15 min, required amount of DEAEEMA (Table S1) was added along with 1 mL of 0.01 (N) HCl and reaction was continued up to 3 h at the same temperature and stirring speed. Subsequently, the copolymerization reaction was terminated using saturated solution of hydroquinone. Then the reaction mixture was cooled to room temperature and precipitated with methanol/water mixture followed by acetone (400 mL) to remove unreacted monomer and homopolymer (if formed). Finally, the product was dried in a vacuum oven at 60°C.

**Table S1.** Synthesis details of AP-g-p(DEAEEMA).

Polymer	Initiator conc. (mole $\times 10^{-5}$ )	Monomer conc. (mole)	% G <sup>a</sup>
AP-g-p(DEAEEMA)-1	0.554	0.0248	51.05
AP-g-p(DEAEEMA)-2	1.294	0.0248	65.12
AP-g-p(DEAEEMA)-3	2.034	0.0248	76.25
AP-g-p(DEAEEMA)-4	2.774	0.0248	84.07
AP-g-p(DEAEEMA)-5	3.514	0.0248	72.36
AP-g-p(DEAEEMA)-6	2.774	0.0373	62.24
AP-g-p(DEAEEMA)-7	2.774	0.0124	46.15

$${}^a \text{ \% grafting} = \frac{\text{wt. of graft co-polymer} - \text{wt. of polysaccharide}}{\text{wt. of polysaccharide}} \times 100$$

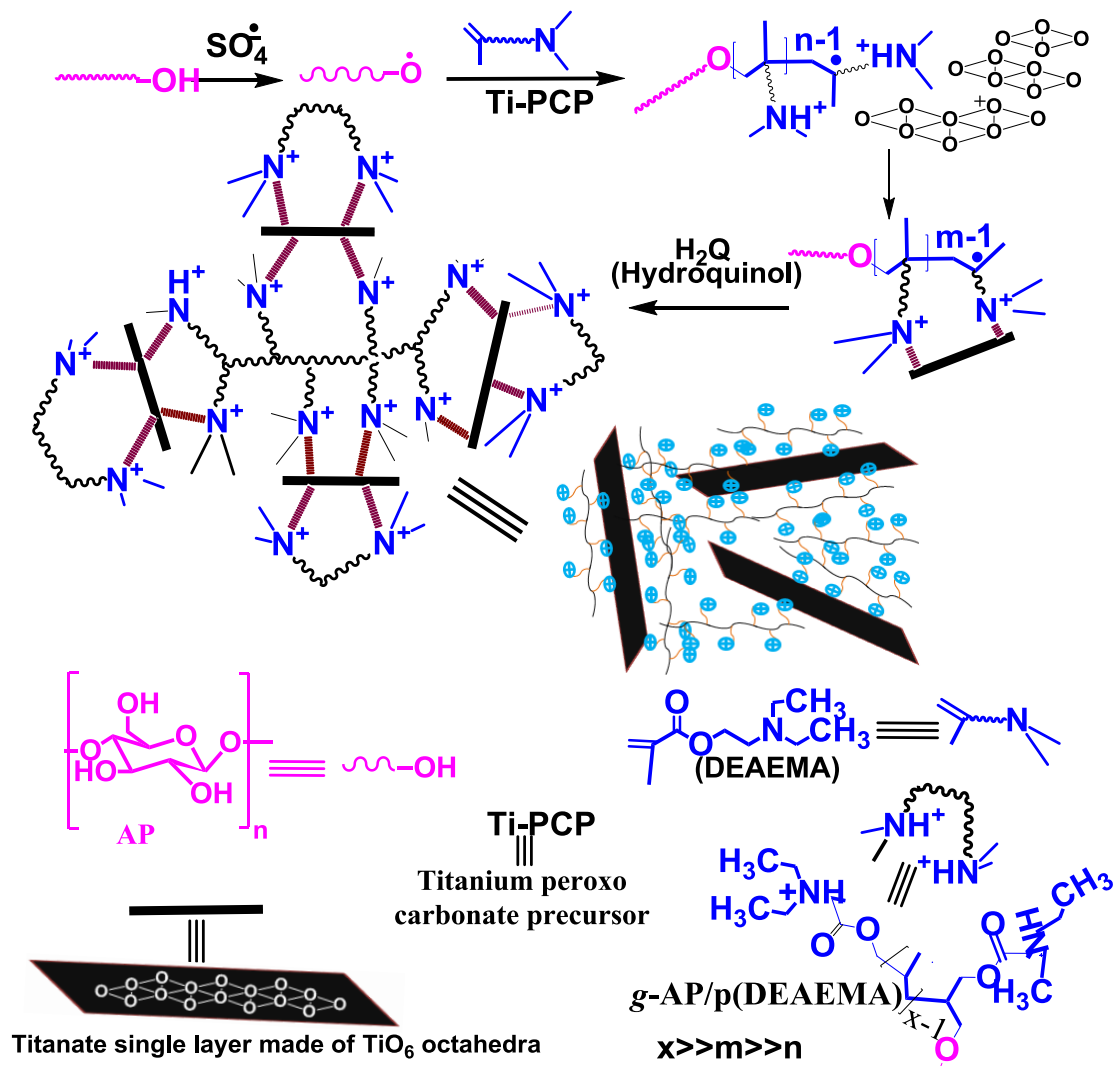
### ***Synthesis of exf.LT/AP-g-p(DEAEEMA):***

The *exf.LT/AP-g-p(DEAEEMA)* was synthesized by following way:

10 mL of dry ethanol was taken in a 100 mL beaker. Then 0.01 mole of titanium isopropoxide was added and was dissolved by continuous stirring at 500 rpm. In due course, just after the addition of 40 mL of ammonical water, a white precipitate was appeared. The stirring was

continued up to 15 min and the precipitate was collected by centrifugation. Then the precipitate was washed for 4 times with double distilled water. An aqueous solution of ammonium carbonate (25mL, 1.6 M) was added to the precipitate with constant stirring followed by addition of 3 mL of 30% H<sub>2</sub>O<sub>2</sub>.<sup>2</sup> The stirring was continued for half an hour at reflux condition.

In another section, the graft copolymerization of *poly* (DEAEMA) on amylopectin backbone was carried out as explained before. Once the colour of the polymerization mixture became milky white, then titanium peroxo carbonate solution (which was stirred for half an hour) was added into the reaction mixture. Afterwards, the reaction was continued up to 3 h at 80°C with constant stirring. Then the reaction mixture was precipitated by adding 400 mL of methanol/water followed by acetone. The product was recovered via vacuum filtration and dried under vacuum at 60°C for overnight.



**Scheme S1.** Schematic representation for the synthesis of fully exfoliated titanate layered- AP-g-p(DEAEMA) nanocomposite i.e. *exf.LT/AP-g-p(DEAEMA)*.

***Synthesis of ex-situ CTAB stabilized layered titanate sheet incorporated graft copolymer [CTAB exf.LT/AP-g-p(DEAEMA)]:***

0.03 mole CTAB was added into 30 mL water and was dissolved at 50°C with continuous stirring of 500 rpm. Then 10 mL of 1.6 M ammonium carbonate was added on the CTAB solution. Afterwards, freshly prepared ammonium peroxy carbonate (using 0.01 mole of titanium precursor) solution was added into the aqueous solution of CTAB. Afterwards, the total system was placed into reflux condition for 2 h (CTAB-LT). In another section amylopectin with optimized concentration of KPS/DEAEMA (see [Table S1](#)) was added in 3 necked RB with continuous N<sub>2</sub> purging. Just after 15 min, refluxed CTAB-LT was added on to the amylopectin solution in N<sub>2</sub> environment. Then the reaction was continued up to 3 h 80° C. Subsequently the whole reaction mixture was cooled to room temperature. Then the reaction mixture was precipitated by adding 400 mL of acetone. Finally, the product was dried at 60°C in a vacuum oven.

***Synthesis of ex-situ incorporation of layered titanate in AP-g-p(DEAEMA) [LT/AP-g-p(DEAEMA)]:***

Freshly prepared titanium peroxy carbonate solution was refluxed for 2 h. Then the solution was mixed with the amylopectin solution in a 3 necked RB, followed by nitrogen purging. After that, optimized concentration of KPS/DEAEMA (see [Table S1](#)) was added to the reaction mixture and the reaction was continued at 80°C for 3 h under inert atmosphere of nitrogen. Finally, the reaction mixture was cooled to room temperature, precipitated in acetone and dried in a vacuum oven at 60°C.

## **CHARACTERIZATION:**

FTIR spectra were recorded using FTIR spectrometer (Perkin Elmer, Model Spectrum 2000) using KBr pellet method with scan range of 400 to 4000  $\text{cm}^{-1}$ .

Solid state  $^{13}\text{C}$ -NMR spectra were recorded at 500MHz on a Bruker Advance II-500NMR spectrophotometer.

Thermogravimetric analysis was carried out with a TGA analyzer (Model – STA449F3, Netzsch, Germany) in presence of inert atmosphere of nitrogen. The heating rate was 5  $^{\circ}\text{C}/\text{min}$ .

The surface morphology was analyzed using field emission scanning electron microscopy (FESEM Supra 55, Make - Zeiss, Germany) and High Resolution Transmission Electron Microscope (JEOL JEM 2100 microscope).

Powder X-ray diffraction (XRD) spectra were recorded using Bruker X-ray diffractometer (Bruker, D8-Focus, Germany).

Surface topography was analysed using atomic force microscopy (AFM, Dimension Icon Multimode 5, Bruker, Germany).

Photocatalytic degradation was carried out using a UV chamber (made: REMCO, INDIA).

Specific surface area was calculated using surface area analyzer (NOVA 3200e, Quantachrome, USA) at liquid nitrogen temperature 77 K.

Surface potential and particle size distribution of the composite were measured using zeta sizer Nano ZS (Malvern, UK).

## **ADSORPTION STUDY:**

1000  $\text{mg. L}^{-1}$  of stock solutions for MB, MG, RB, MO dyes were prepared and further diluted to different experimental concentrations. Batch experiments were studied using orbital shaker (Rivotek, Kolkata, India). The experiments were performed with varying solution pH, contact

time, initial dye concentration and adsorbent dosage. In 100 mL of aliquot, required amount of exf.LT/AP-g-p(DEAEMA) was added. At a desired time interval, supernatant solution was collected through centrifugation. The dye concentration of each experimental solution before and after adsorption was evaluated using a calibration curve plotted in UV-Vis spectroscopy. The % removal of dye was determined using  $(C_0 - C_e)/C_0 \times 100 \%$  and at equilibrium the amount of dye adsorbed was evaluated by  $(C_0 - C_e) \times V/W$ , Where  $C_0$  ( $\text{mg L}^{-1}$ ) and  $C_e$  ( $\text{mg L}^{-1}$ ) are the initial and final concentration of dye solutions, respectively. V (mL) and W (g) are the volume of the dye solution and the weight of the exf.LT/AP-g-p(DEAEMA), respectively.

### ***Selective adsorption of cationic and anionic dyes:***

The selective separation of cationic and anionic dyes from mixture of dyes is very essential from industrial point of view.<sup>3</sup> The selective removal of individual dyes from mixture of dye solution was carried out at optimum condition. Individual stock solutions of MB ( $10 \text{ mg L}^{-1}$ ), MG ( $10 \text{ mg L}^{-1}$ ), MO ( $10 \text{ mg L}^{-1}$ ), RB ( $10 \text{ mg L}^{-1}$ ) were prepared in 100 mL volumetric flask. These solutions were categorized into two different mixtures of dye solutions. The dye solutions were considered as mixture 1 (MO and MB) and mixture 2 (MO and MG), respectively. 25 mL of dye mixture was taken for analysis. The selective removal was performed for mixture 1 and mixture 2 at their corresponding optimized condition. After centrifugation, the sample solutions were analyzed using UV-Vis spectrophotometer.

### ***Photocatalytic degradation:***

To determine the photocatalytic degradation efficiency of exf. LT/AP-g-p(DEAEMA), 50 mL of each MO/MB aqueous solutions were taken for study. 15 mg of exf. LT/AP-g-p(DEAEMA) was added on dye (MO/MB) solution and left it for 30 min in dark with continuous stirring to equilibrate. After that the solution was placed under UV chamber ( $\lambda = 355 \text{ nm}$ ) (made: REMCO,

Kolkata, India). After fixed irradiation time, 3 mL of dye solution was withdrawn and centrifuged. The supernatant solution was used to investigate the change in MO/MB concentrations using UV-visible spectrophotometer (Make: Shimadzu, Japan; Model: UV 1800).

### ***Regeneration Study via desorption and degradation:***

Desorption phenomenon is exactly opposite to adsorption. An efficient adsorbent should have both adsorption and desorption characteristics.<sup>4</sup> Desorption is a process in which adsorbed material was released from the surface of adsorbent. However, in dye desorption process the toxic dyes became reenter on to the environment. Besides, exudation of dye wastewater is a real threat to mankind. Accordingly the possibility of reuse of synthetic dye wastewater should be neglected due to environmental strategy. A complete removal of dye can be possible via adsorption as well as degradation process.<sup>5</sup> Adsorbed dye was desorbed by maintaining the pH of respective dye solutions. For desorption study optimized dye concentration of cationic (MO, RB) and anionic (MB, MG) dyes were used. Weighed amount of adsorbent was added into the dye solutions. Stripping solutions with pH-2.5, 7, 10.5 were taken for desorption study. Desorption study was continued until the whole dye became in solution phase. For regeneration of adsorbent via degradation, the respective dye loaded composite was placed in a continuous exposure of UV light (355 nm). After degradation, composite was collected and then adsorption study was done followed by degradation in UV light for consecutive five cycles.

## **S2: RESULTS AND DISCUSSIONS**

### ***Solid state <sup>13</sup>C NMR spectra:***

Solid state <sup>13</sup>C NMR spectrum of AP-g-p(DEAEMA) showed few additional peaks corresponding to amylopectin.<sup>6</sup> The peaks at  $\delta= 103.6, 83.4, 73.4$  and  $64.2$  ppm are attributed for anomeric carbon atom, for carbon atoms of C-2 to C-4 (except anomeric carbon atom), for -

CH<sub>2</sub>OH carbon atom and C-5 carbon atom. The peak at 57.4 ppm was due to presence of the carbon moiety attached with ester oxygen group in AP-g-p(DEAEMA). Peaks at 13.6 and 17.2 ppm are characteristics peaks of methylene and methyl carbon of the grafted moiety, respectively. Peaks at 45.7 and 49.1 ppm are attributed to sp<sup>3</sup> hybridized carbon atoms, which were formed during the polymerization of DEAEMA (see [Scheme 1](#)). Moreover, the additional peak at 177.2 ppm predicts the occurrence of carbonyl carbon of ester. The presence of these additional peaks confirmed the formation of graft copolymer ([Fig. S1a](#)). Besides, the <sup>13</sup>C NMR spectrum of exf.LT/AP-g-p(DEAEMA) ([Fig. S1b](#)) reveals that all the characteristics peaks are present. However, the peak value was shifted towards higher region (downfield shift). This observation further confirms that electrostatic interactions predominate between anionic titanate sheet and cationic AP-g-p(DEAEMA) in the fully exfoliated nanocomposite.

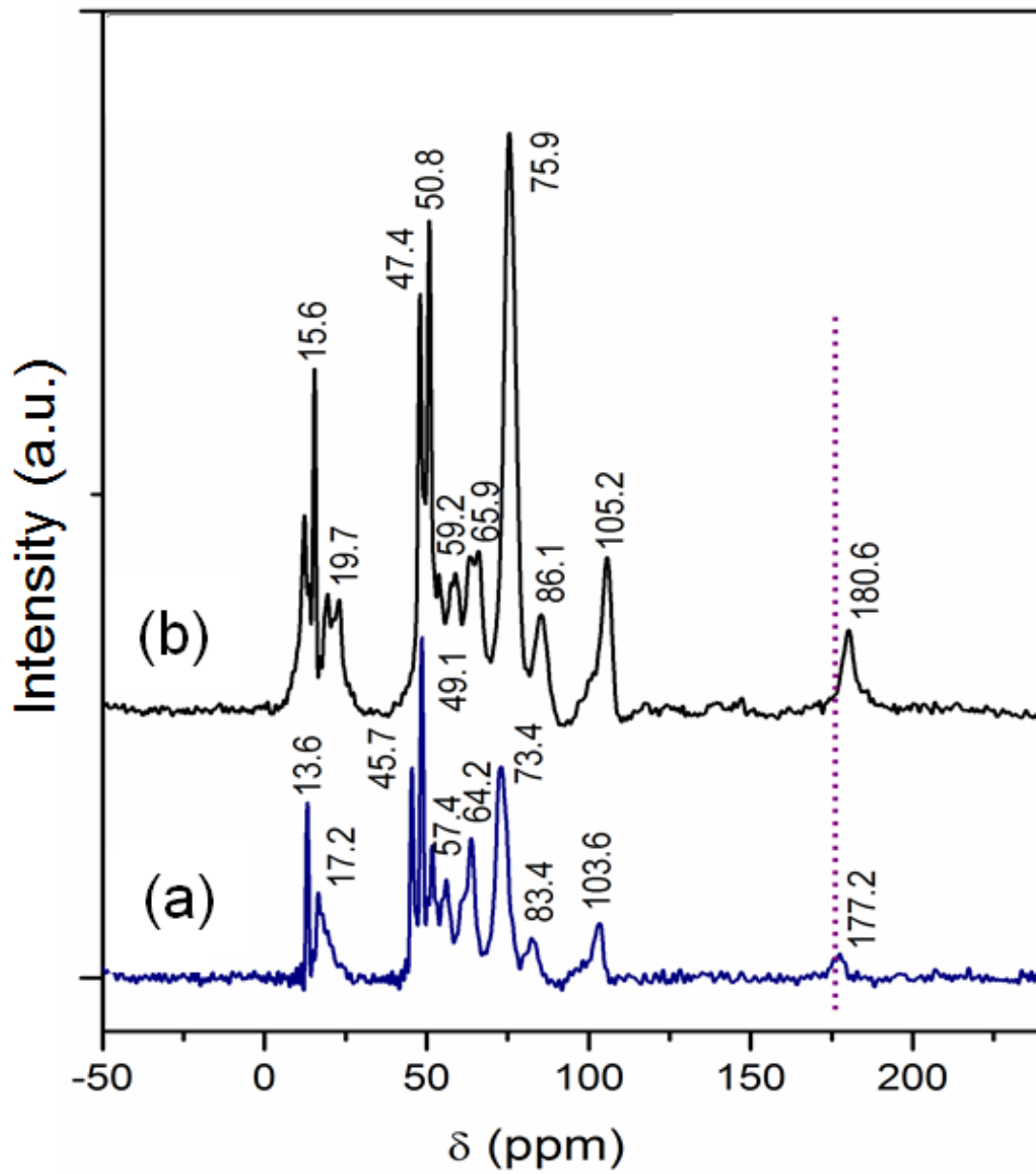


**Fig. S1.** Solid-state  $^{13}\text{C}$  NMR spectra of (a) pure AP-g-p(DEAEMA) and (b) exf.LT/AP-g-p(DEAEMA) nanocomposite

**FTIR spectra:**

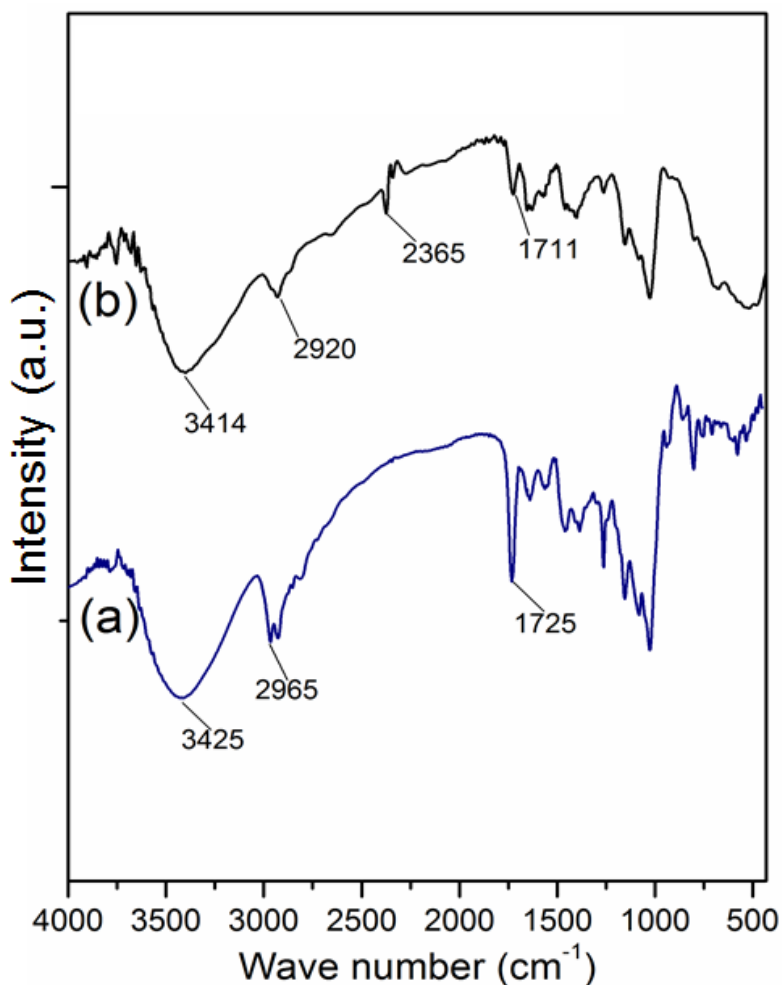


**Fig.S2.** FT-IR spectra of (a) pure AP-g- p(DEAEMA) and (b) exf.LT/AP-g-p(DEAEMA) nanocomposite

FTIR spectrum of AP-g-p(DEAEMA) (Fig. S2a) predicts that all the characteristic peaks of amylopectin were present.<sup>7</sup> Besides, an intense peak at 1725 cm<sup>-1</sup> was observed which is due to the ester carbonyl of *poly* (DEAEMA). This observation suggests that DEAEMA has been grafted onto amylopectin backbone. The FTIR spectrum of exf.LT/AP-g-p(DEAEMA) (Fig S2 b) demonstrates the same characteristic peaks along with an additional peak at 2365 cm<sup>-1</sup>, which is attributed for the formation of –OH chelated compound (i.e. titanium peroxo carbonate). It is presumed that an electrostatic interaction was established between exfoliated single layered sheet

and cationic AP-g-p(DEAEMA). The shifting of peak positions with lower intensity along with the formation of  $-OH$  chelated complex further confirmed the observation. A broad band at around  $3430\text{ cm}^{-1}$  was shifted to  $3400\text{ cm}^{-1}$  and the characteristics peak of ester carbonyl was also shifted from  $1725$  to  $1711\text{ cm}^{-1}$ . Thus from above observations, it can be stated that electrostatic interactions were involved between the negatively charged titanate sheet and positively charged AP-g-p(DEAEMA) for fully exfoliation process.

***FE-SEM analysis:***

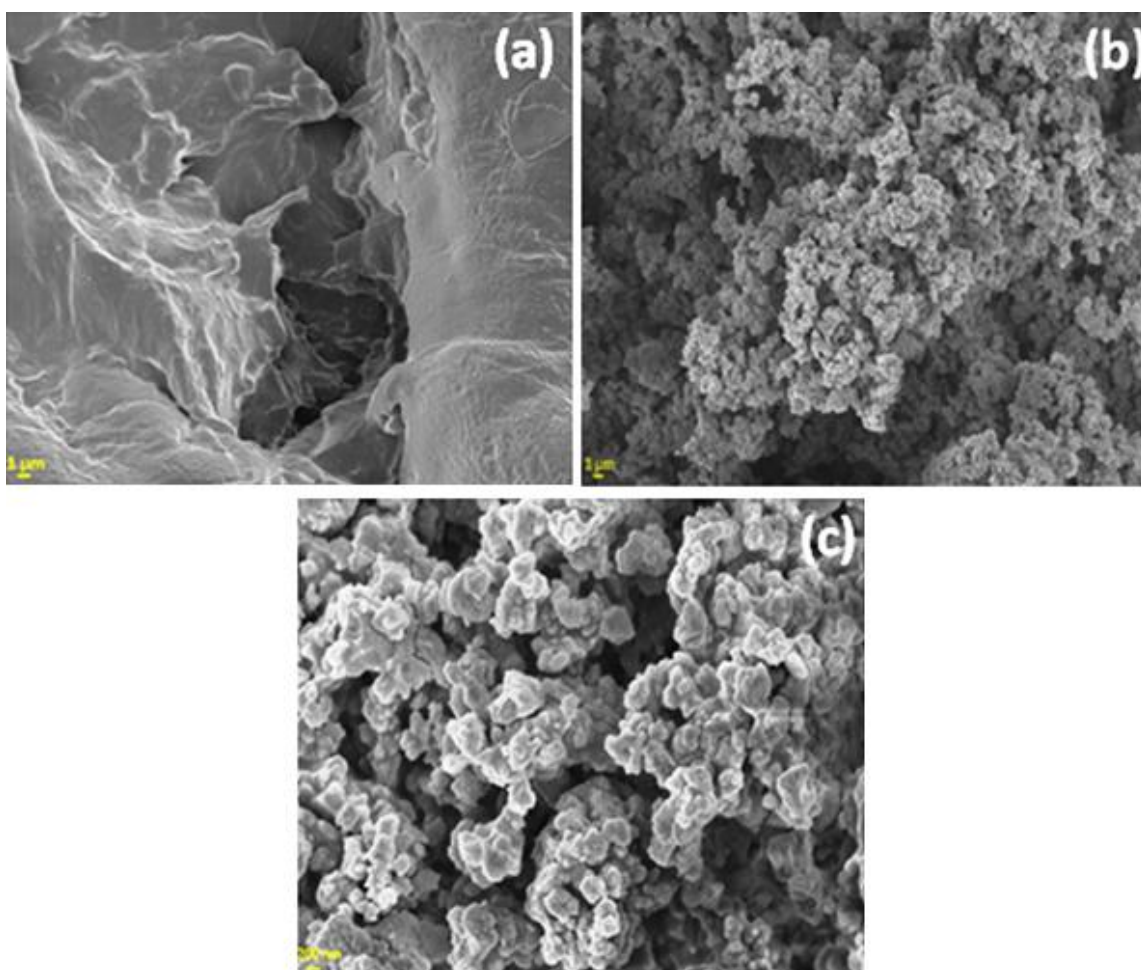


**Fig. S3.** FE-SEM images of (a) pure AP-g- p(DEAEMA), (b) exf.LT/AP-g-p(DEAEMA) nanocomposite and (c) closer view of exf.LT/AP-g-p(DEAEMA)

*AFM analysis:*

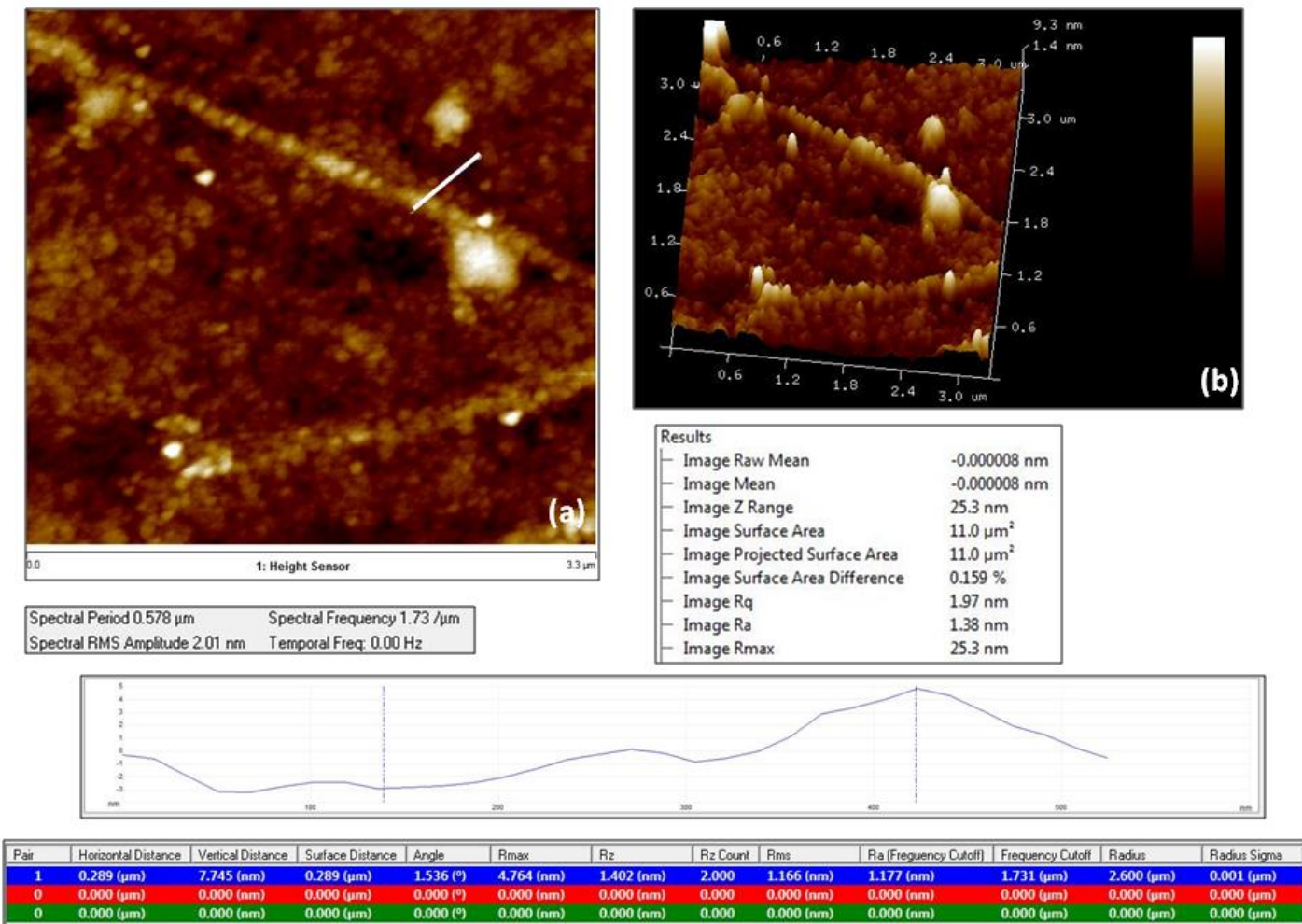


**Fig. S4.** (a) Height sensor and (b) 3D-image of exf.LT/AP-g-p(DEAEMA)

*EDAX analysis:*

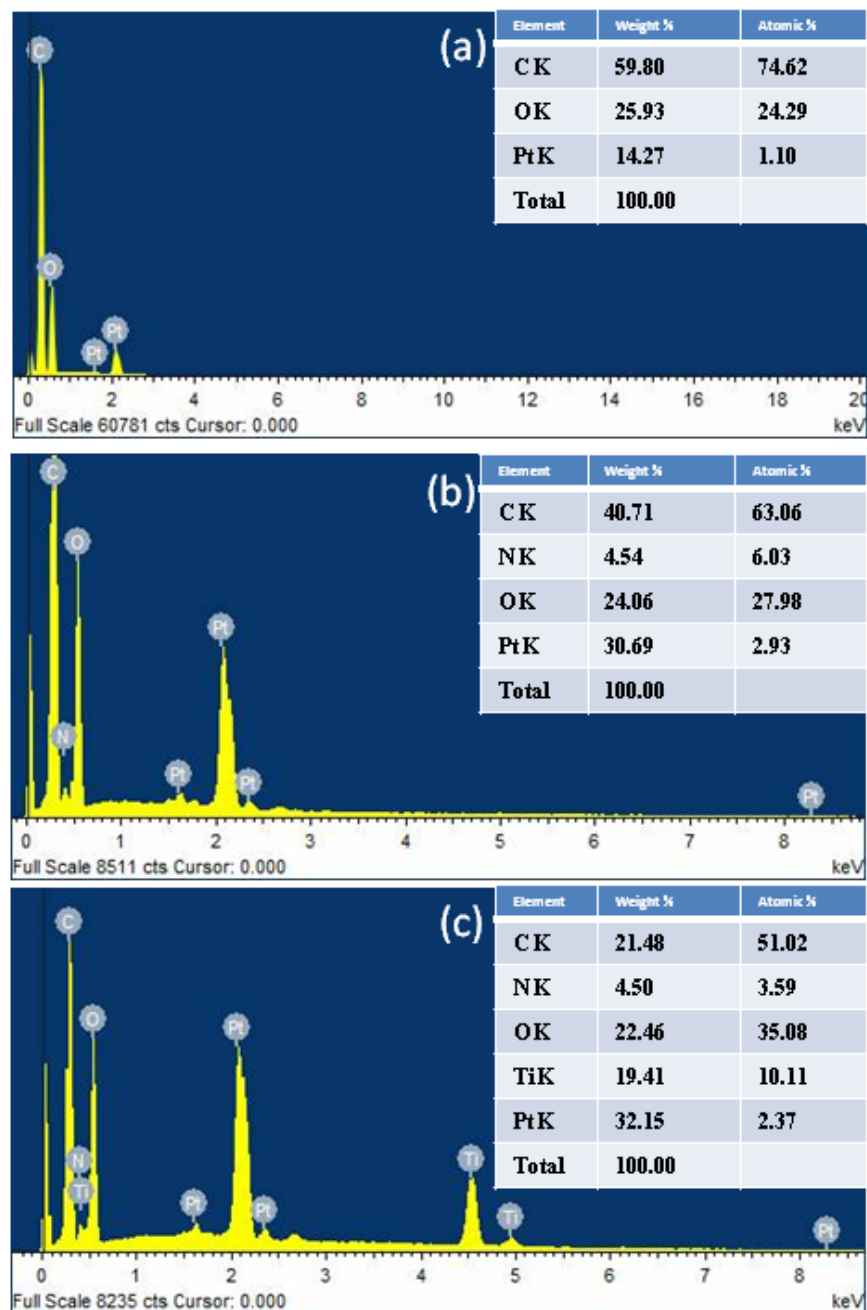


**Fig. S5.** EDAX spectra of (a) AP, (b) AP-g-p(DEAEMA), and (c) exf.LT/AP-g-p(DEAEMA)

### TGA analysis:

Fig. S6 illustrates the comparative TGA analysis of AP-g-p(DEAEMA) and *exf.LT/AP-g-p*(DEAEMA). The three stage degradation zones were observed for AP-g-p(DEAEMA). Initial weight loss (50-100 °C) occurred due to loss of moisture. The second degradation zone was observed between 250-330 °C. This is probably due to the decomposition of polysaccharide backbone. The weight loss region in the range of 340-460 °C is attributed to the degradation of grafted *poly* (DEAEMA) chains. The TGA curve of *exf.LT/AP-g-p*(DEAEMA) exhibits all the three stages of degradation regions. However, it was observed that stability range increased for each mass loss region. Besides, an additional weight loss region was attributed in the range of 490-1200 °C. This weight loss zone is probably owing to the decomposition of large number of interacting cationic moieties with exfoliated titanate nano sheet. The similar enhancement of thermal stability was found in organic- inorganic nanocomposite.<sup>8</sup>

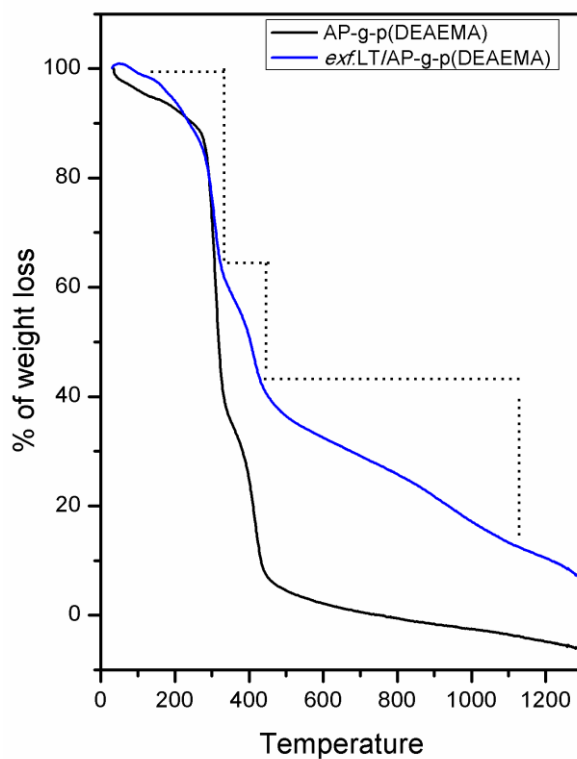


**Fig. S6.** TGA plots of pure AP-g- p(DEAEMA) and *exf.LT/AP-g-p*(DEAEMA) composite

### *XRD analysis:*

In the XRD pattern of exf.LT/AP-g-p(DEAEMA) composite (Fig. S7), diffraction peak for layered structure ( $2\theta=9.7$ ) was absent and suggests the absence of stacked titanate layers. Presence of other low intense peaks for titanate sheets directs the presence of titanate sheets in the composite (inset). The low instance noisy peaks are due to the presence of large amount amorphous polymeric compounds.

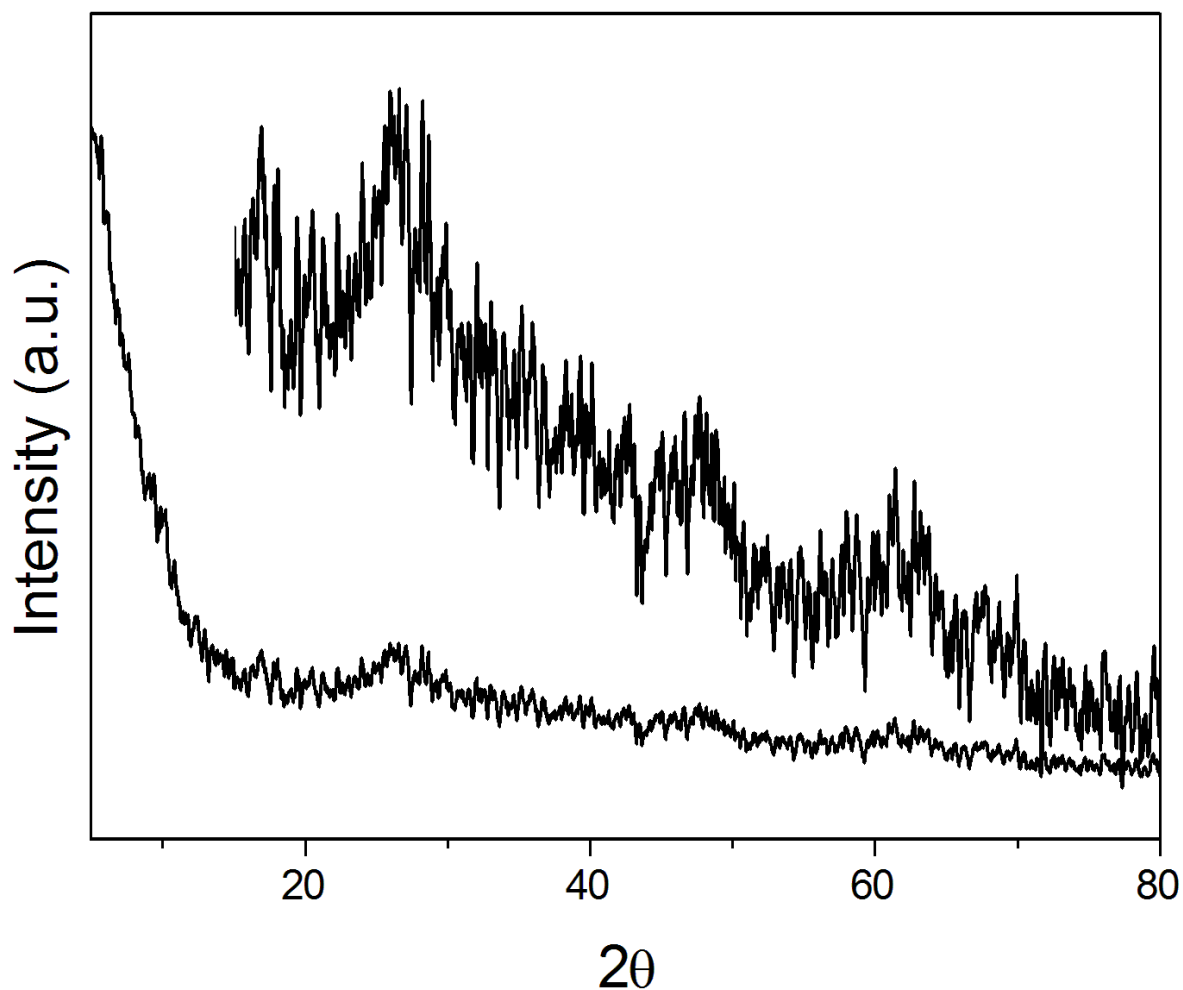


**Figure S7.** XRD pattern of synthesized exf.LT/AP-g-p(DEAEMA)

***HR-TEM analysis:***

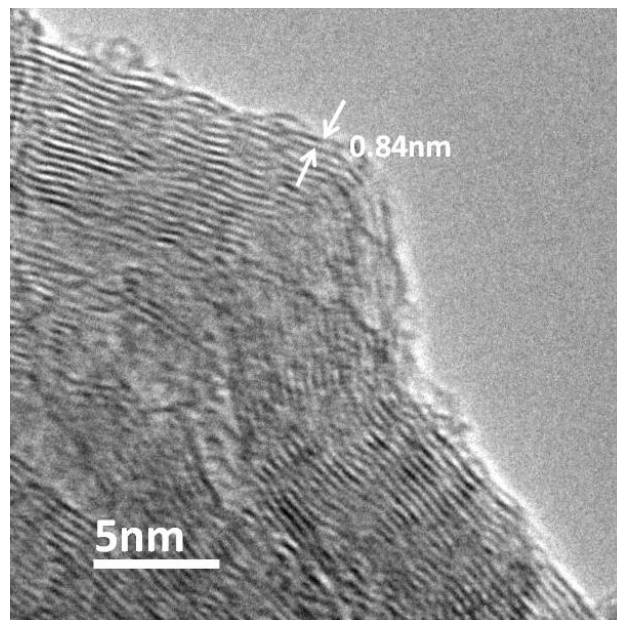


**Fig. S8.** TEM image of pure layer titanate synthesized at the temperature 80°C at which the composite were synthesized

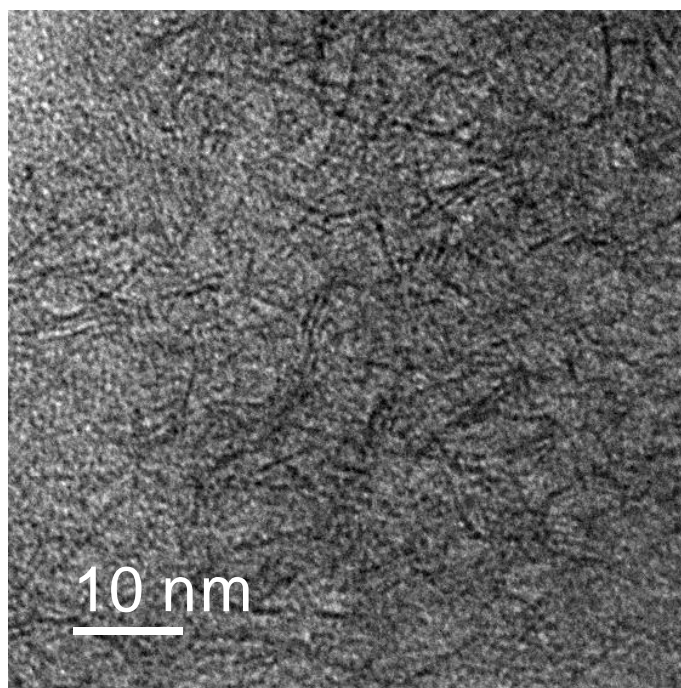


**Figure S9.** TEM image of synthesized exf.LT/AP-g-p(DEAEMA) composite

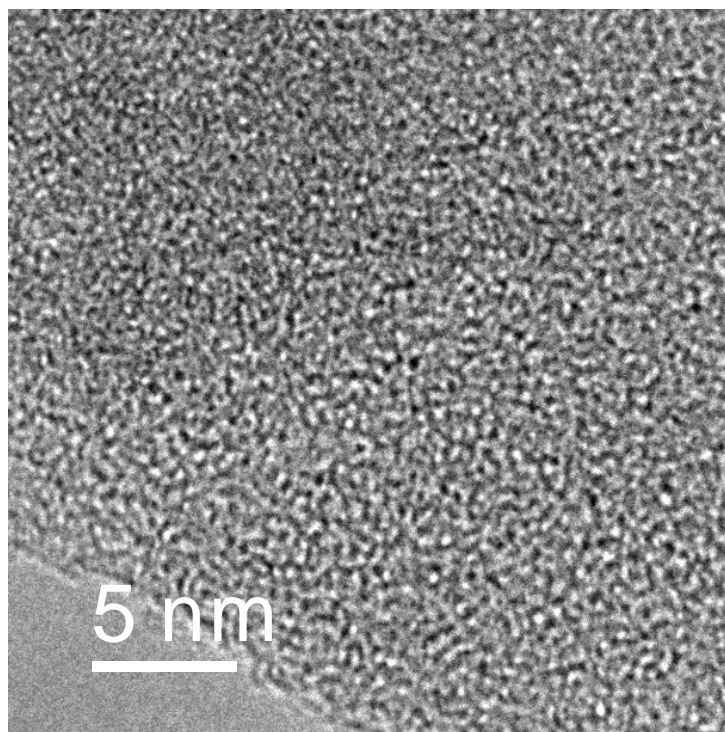


**Fig. S10.** TEM image of synthesized *pure* AP-g- p(DEAEMA) graft copolymer

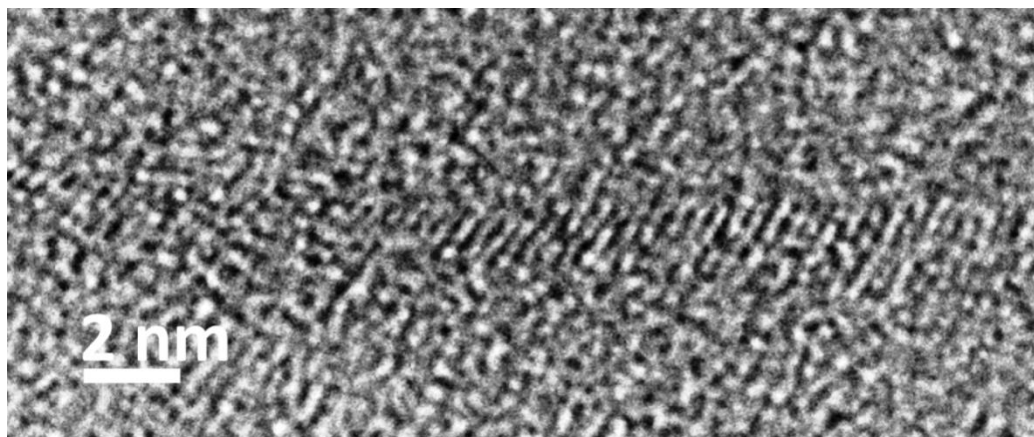


**Fig. S11.** HR-TEM image of synthesized exf.LT/AP-g-p(DEAEMA), depicting the lattice fringes of head (wire like, as seen in TEM images) of the titanate sheets

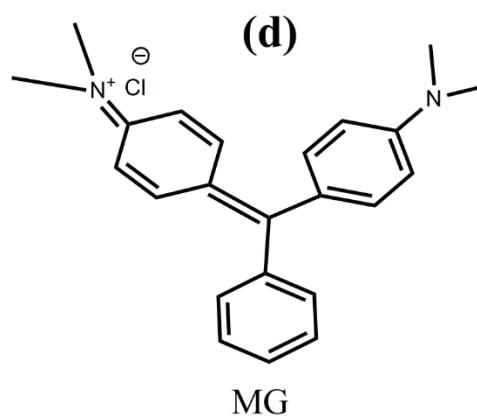
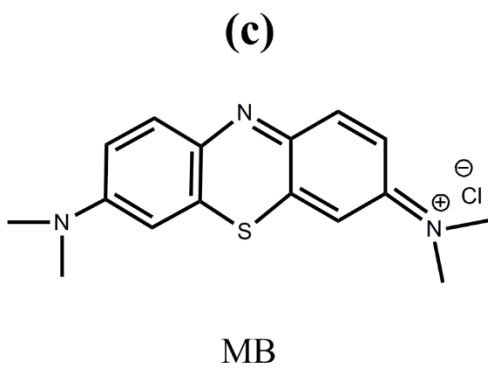
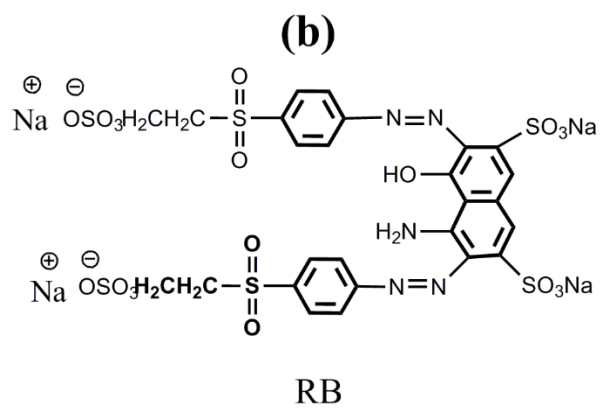
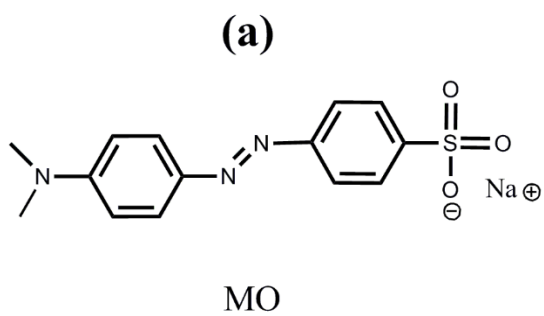


**Fig. S12.** Molecular structures of (a) MO, (b) RB, (c) MB and (d) MG dyes

## ADSORPTION OPTIMIZATIONS:

Removal of cationic (MB, MG) and anionic (MO, RB) dyes from aqueous solution depends on the solution pH, contact time, temperature, adsorbent dosage and dye concentration. All the parameters were optimized to have the best adsorption condition.

### *Effect of pH:*

The key concept of the adsorption characteristics is dependent on *pH* responsive behavior of *poly*[2-(diethylamino)ethyl methacrylate] i.e. *poly* (DEAEMA). Huang *et al.* reported that cross linked DEAEMA have excellent swelling behavior depending upon pH of the solution.<sup>9</sup> *exf.LT/AP-g-p*(DEAEMA) was insoluble in entire pH range of 3-10. However, it was observed that at  $\text{pH} < 4.4$ , better swelling property was observed. This is because at  $\text{pH} < 4.4$  ( $\text{pH} < \text{pH}_{\text{pzc}}$ ), the entangled chain of *poly* (DEAEMA) was protonated. Accordingly the repulsive interactions between the protonated chains attributed to stretched conformation, which would absorb large amount of water. In addition, it is presumed that electrostatic interactions between AP-g-p(DEAEMA) and layered sheet of titanium makes the composite material insoluble at entire pH region. But, at higher pH, the protonated chain became deprotonated and the stretched conformation was collapsed. The pH of experimental dye solution has strong effect on active sites of adsorbent as well as ionization of dye solution. The effect of solution pH on the removal of anionic RB/MO and cationic MB/MG has been reported by varying the pH of aqueous media. In case of anionic dyes (Fig. S13a), the % adsorption decreased with increase in pH from 3 to 6 and beyond which it was in plateau. At acidic media, exfoliated single titanate sheet was covered up with highly stretched AP-g-p(DEAEMA). Thus, interacted area was increased for an efficient adsorption process. Therefore, the stretched AP-g-p(DEAEMA) on single sheet of titanate could hold excess amount of anionic RB/MO dyes. Besides at acidic pH, adsorbent surface became

positively charged while the adsorbate is in negatively ionized form, which revealed maximum % of RB/MO dyes removal.

At basic pH, the stretched protonated chain of AP-*g*-p(DEAEMA) became deprotonated. So, the stretched confirmation of *poly* (DEAEMA) was collapsed followed by negatively charged titanate sheets are free to bind with cationic dyes (MB, MG) at basic condition. The effect of pH for MB/MG dyes was studied by varying the pH of media from 6 to 10 for both MB/MG dyes (Fig. S13b). For both cases, it has been observed that after pH-8, the dye removal was efficient compared to acidic condition. Under alkaline condition, because of the enhancement of excess negatively charge on adsorbent surface, the electrostatic attraction became predominant. This result in an increase in % removal of cationic dyes. These observations can be explained on the basis of the formation of an ionic complex between cationic dye and negatively charged surface of exfoliated layer titanate.

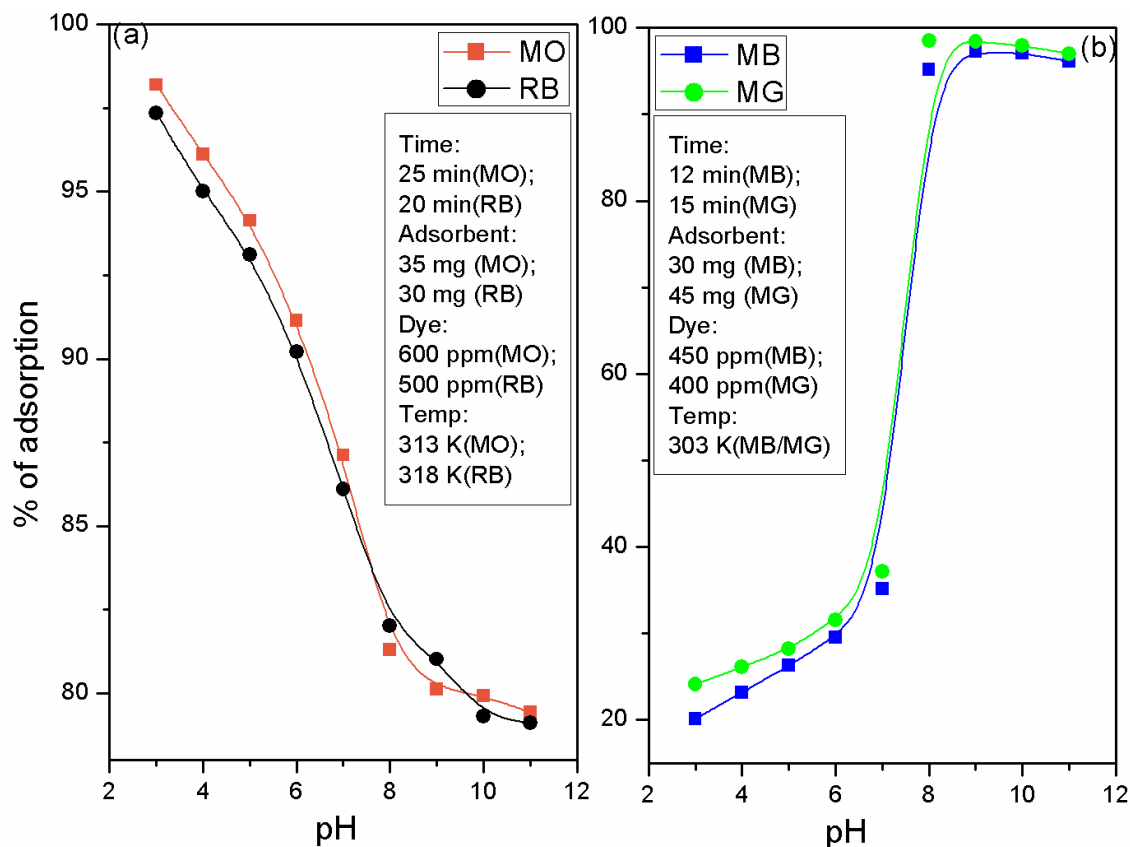


**Fig. S13.** Effect of pH on % adsorption of (a) MO/RB and (b) MB/MG dyes using exf.LT/AP-g-p(DEAEMA)

***Effect of contact time:***

The adsorption study was performed with variable contact time for MO, RB, MG, MB dyes. Fig.S14 demonstrates that initially rate of dye uptake was increased with increase in time for both cationic and anionic dyes. At pH3, ~ 98.20 % of MO and ~ 97.35 % of RB were removed within 25 and 20 min, respectively. At pH9, ~ 97.26% of MB removal was occurred within 12 min and at pH8, ~98.50 % MG removal was obtained within 15 min. Afterwards, the removal rate was almost constant. Thus the efficient and rapid adsorption revealed that a quick monolayer formation was occurred on the external surface of adsorbent. Basically in both cases at their respective pH, a rapid adsorption of dye removal was observed followed by it was controlled through mass transport in the exf.LT/AP-g-p(DEAEMA).

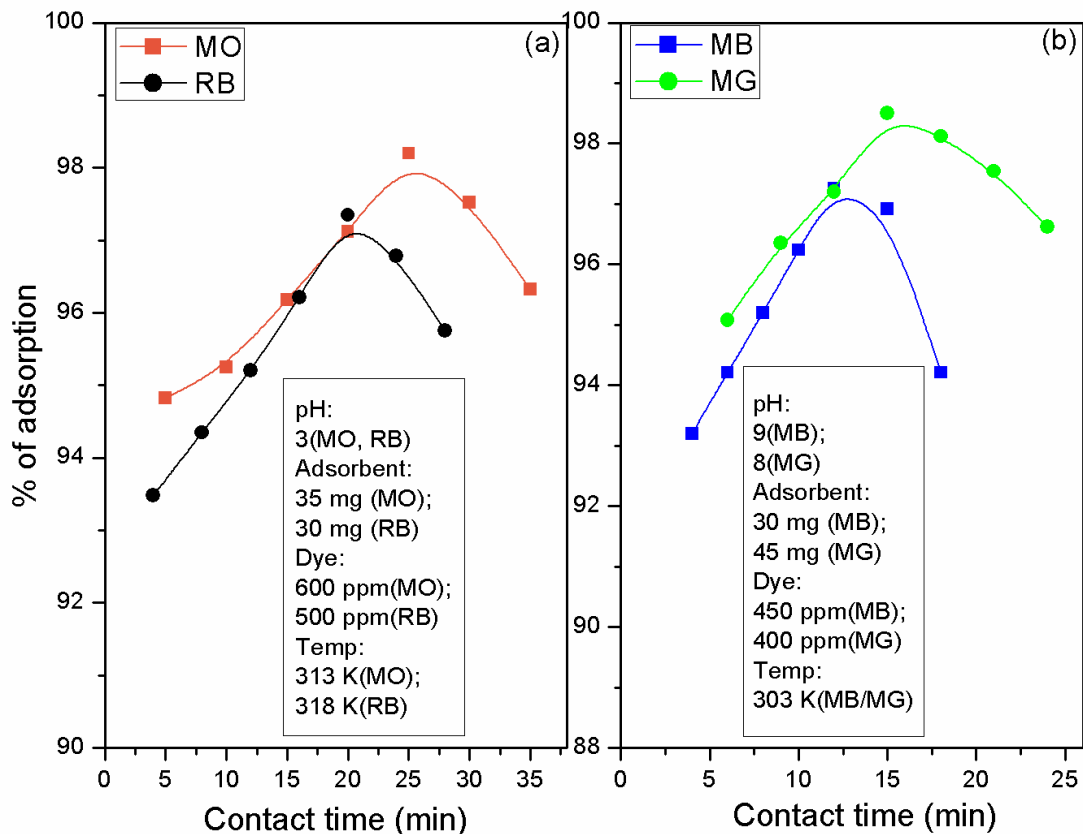


**Fig. S14.**Effect of contact time on % adsorption of (a) MO/RB and (b) MB/MG dyes using *exf.LT/AP-g-p(DEAEMA)*

***Effect of adsorbent dosage:***

The amount of adsorbent dosage (mg) played a crucial role in dye removal process. The optimized adsorbent dosages are 35 mg for MO, 30 mg for RB, 30 mg for MB and 45 mg for MG. That optimum dosages were required for removal of maximum % of dyes and after that the removal was declined (Fig. S15). The availability of active sites on *exf.LT/AP-g-p(DEAEMA)* has played an effective role in rapid adsorption process. Higher adsorbent dosage caused aggregation of surface active sites to enhance the diffusion path length. Thus the reduced available surface active sites would result in lower % of dye removal.

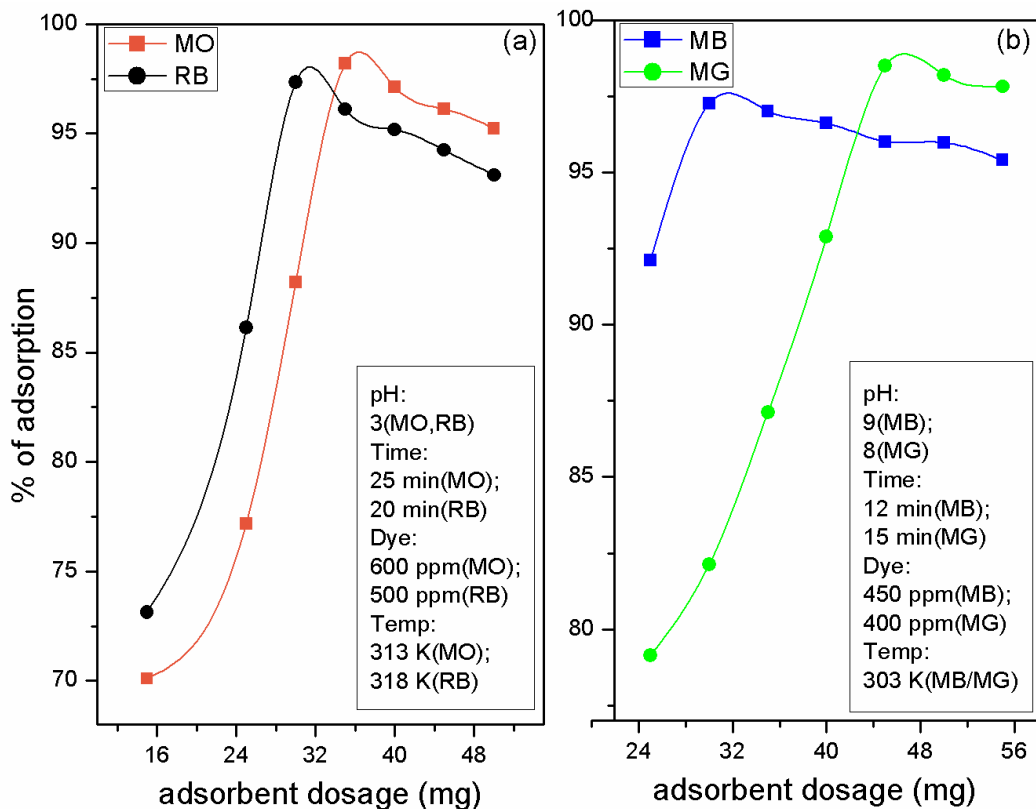


**Fig. S15.** Effect of adsorbent dosage on the performance of adsorption of (a) MO/RB and (b) MB/MG dyes using *exf.LT/AP-g-p(DEAEMA)*

***Effect of dye concentration:***

[Fig.S16](#) demonstrates that different optimized dye concentrations were responsible for maximum removal of individual MO, RB, MG, MB dyes. Initially with increase in dye concentration, % removal was increased. After that % of dye removal was declined. At lower concentration, maximum number of dye molecules were adsorbed on easily available surface of *exf.LT/AP-g-p(DEAEMA)*. This phenomenon is responsible for higher adsorption efficacy. At higher dye concentration, the saturation of surface active sites was responsible for lower % of dye adsorption.

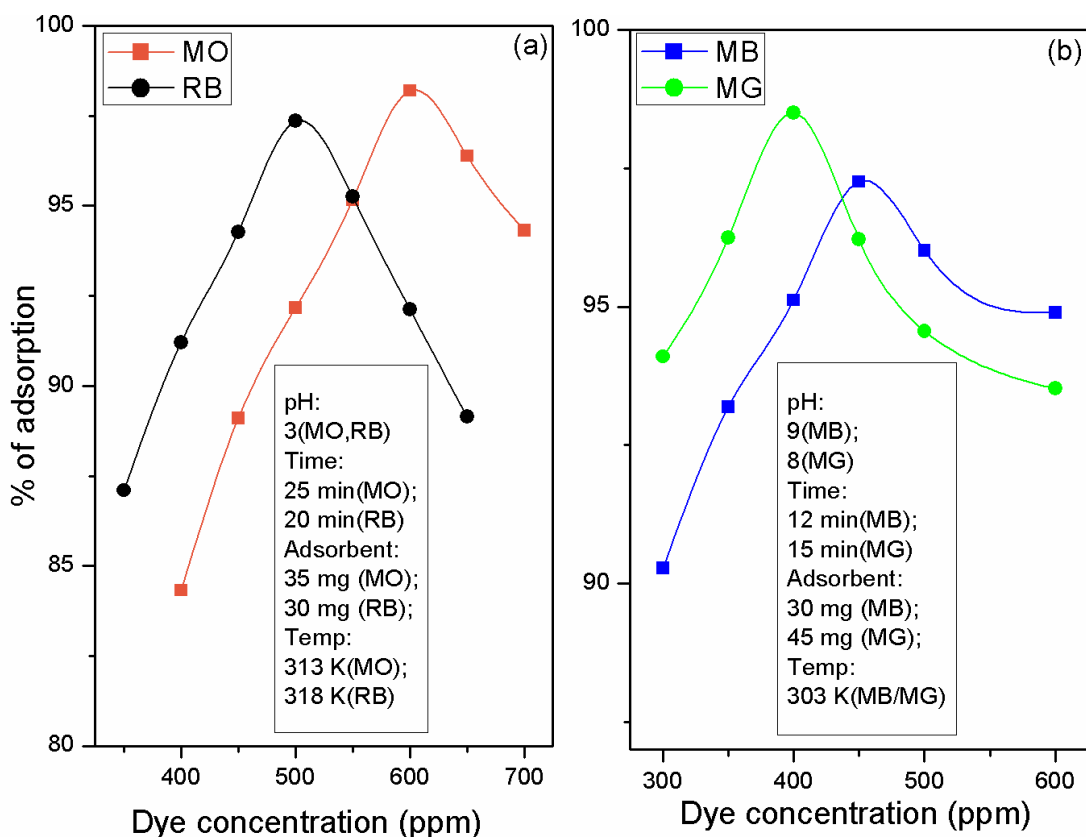


**Fig. S16.** Effect of dye concentration on the performance of adsorption of (a) MO/RB and (b) MB/MG dyes using exf.LT/AP-g-p(DEAEMA)

***Effect of temperature:***

Fig.S17 explains the effect of temperature on removal of MO, RB, MG, MB dyes. For MO/RB dyes, the optimized temperatures were 313K and 318K, respectively. 303 K was optimized temperature for both MB and MG dyes. In both cases, the % of dye removal was increased up to maximum efficiency and after that it was decreased. With increase in temperature the kinetic energy of respective dyes was enhanced and thus dye molecules can properly interact with the available active sites of adsorbent molecule. It has also been noticed that for cationic dyes, relatively higher temperature was required for obtaining higher adsorption efficacy. Swelling is a temperature dependent process and it has important role to channel up the large number of dye

molecules. AP-g-p(DEAEMA) shows a pH responsive swelling effect at acidic media. But at alkaline pH, swelling effect was not observed. Therefore for cationic dyes, relatively lower temperature was required. So, enhancement of kinetic energy with higher temperature was responsible for removal of cationic dyes. Dye uptake capacity was increased with increase in experimental temperature. This clearly revealed that the process was endothermic in nature. This phenomenon further suggests that electrostatic interaction was established between the adsorbate and adsorbent. However, at higher temperature, lower % of dye removal was observed. This was due to the higher mobility of dye molecules, which caused higher rate of desorption.

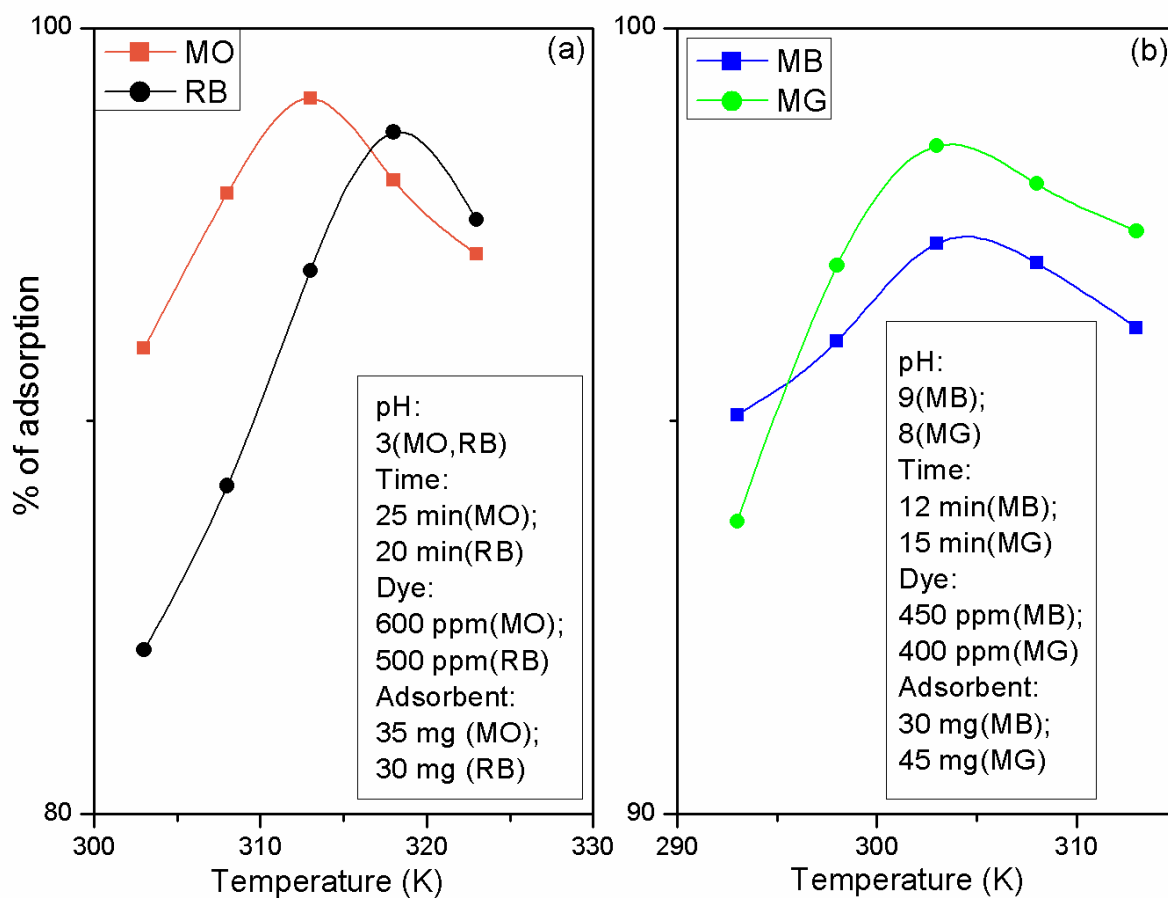


**Fig. S17.** Effect of temperature on the performance of adsorption of (a) MO/RB and (b) MB/MG dyes using *exf.LT/AP-g-p(DEAEMA)*

**Table S2.** Comparison of adsorption capacity of MO, RB, MB, MG using as synthesized adsorbents

Adsorbents	Surface area (m <sup>2</sup> . g <sup>-1</sup> )	Dye	Optimization parameters*	% of adsorption	q <sub>t</sub> (mg.g <sup>-1</sup> )
AP-g-p(DEAEMA)	3.504	MO	pH- 3; CT-40 min; AD- 40 mg; DC-150 ppm; T- 308 K	85.13	79.80
		RB	pH- 3; CT-45 min; AD- 35 mg; DC-125 ppm; T- 313 K	83.13	74.19
		MB	pH- 9; CT-75 min; AD- 40 mg; DC-10 ppm; T-303 K	61.27	3.82
		MG	pH- 3; CT-80 min; AD- 55 mg; DC-10 ppm; T- 303 K	60.32	2.74
CTAB exf.LT/AP-g-p(DEAEMA)	21.510	MO	pH- 3; CT-60 min; AD- 40 mg; DC-300 ppm; T-313 K	89.24	167.25
		RB	pH- 3; CT-50 min; AD- 35 mg; DC-250 ppm; T- 313 K	87.64	156.43
		MB	pH- 9; CT-25 min; AD- 40 mg; DC-250 ppm; T- 303 K	90.01	140.64
		MG	pH- 8; CT-30 min; AD- 50 mg; DC-200 ppm; T- 303 K	88.19	88.19
LT/AP-g-p(DEAEMA)	61.441	MO	pH- 3; CT-60 min; AD- 40 mg; DC-300 ppm; T-313 K	91.34	171.26
		RB	pH- 3; CT-50 min; AD- 35 mg; DC-250 ppm; T-313 K	89.23	159.27
		MB	pH- 9; CT-20 min; AD- 40 mg; DC-250 ppm; T-303 K	92.64	144.75
		MG	pH- 8; CT-25min; AD- 50 mg; DC-200 ppm; T- 303 K	91.25	91.25
exf.LT/AP-g-p(DEAEMA)	125.944	MO	pH- 3; CT-25 min; AD- 35 mg; DC-600 ppm; T- 313 K	98.20	<b>420.68</b>
		RB	pH- 3; CT-20 min; AD- 30 mg; DC-500 ppm; T-318 K	97.35	<b>405.94</b>
		MB	pH- 9; CT-12 min; AD- 30 mg; DC-450 ppm; T-303 K	97.26	<b>365.01</b>
		MG	pH- 8; CT-15 min; AD- 45 mg; DC-400 ppm; T-303 K	98.50	<b>219.06</b>

\* CT= Contact time; AD= Adsorbent dosage; DC= Dye concentration; T= Temperature

## Selective adsorption:

For selective adsorption, mixture 1 (MB and MO) was taken for analysis (Fig. S18). After 5 min, the residual concentration was measured using UV-visible spectrophotometer. It was observed that at pH 3, ~ 12 % of MB dye was adsorbed. In present study, a single titanate sheet was covered up completely by the cationic AP-g-p(DEAEMA). Thus there is no chance of interaction of cationic MB dye with polymer coated single sheet of titanium. Again at pH 9, when MO and MB were used for adsorption study, only 20% MO dye was removed. At pH 9, selective adsorption of cationic dyes occur owing to the coiling of dangling polymeric segments to make negatively charged titanate free for binding selectively with cationic MB or MG dyes. But, it was noticed that when mixture 2 (MO and MG) was taken for selective adsorption, ~ 10 min is required for MG removal at pH-8. This is mainly because of the fact that MG possessed positive charge, which is responsible for selective removal. But in case of MB, positive charge along with a sulphur atom is responsible for selective removal. Similar type of MB removal was observed using dithiol-Protected Ag<sub>7</sub> QuantumCluster.<sup>10</sup>

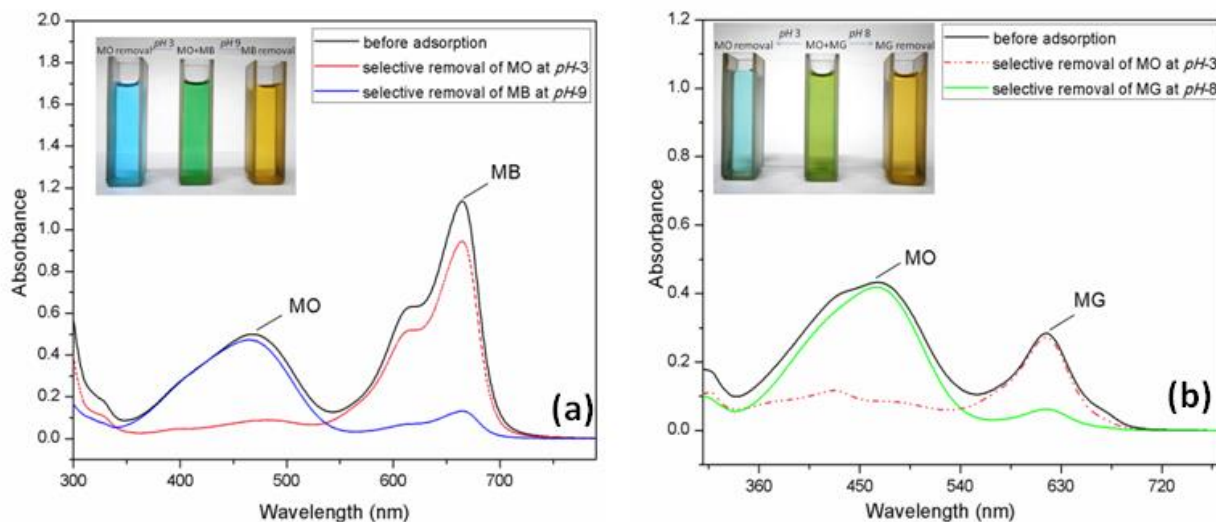


**Fig. S18.** pH responsible selective removal of (a) MB from mixture of MB/MO and (b) MG from mixture of MB/MG

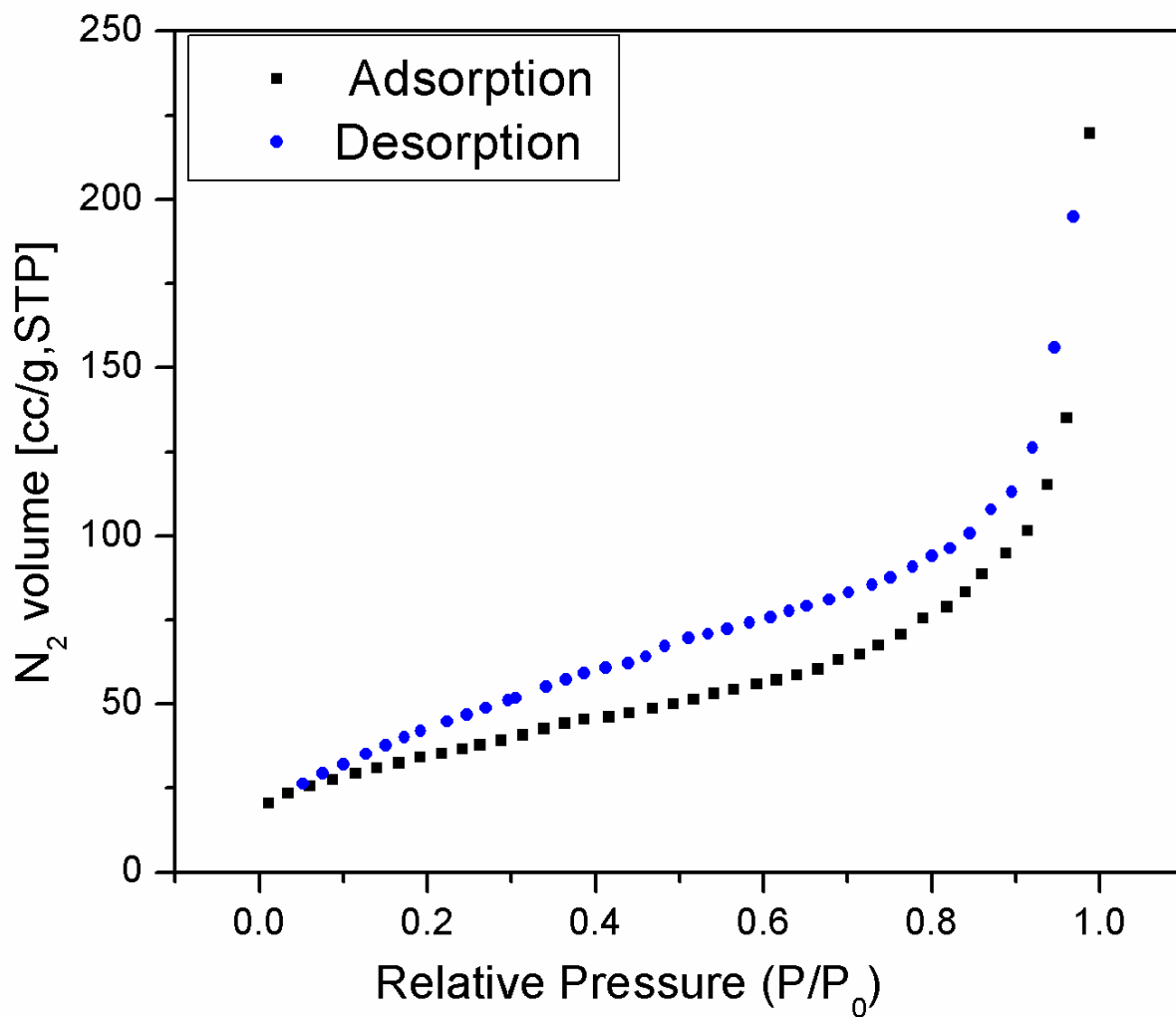


**Fig. S19.** Nitrogen adsorption-desorption isotherms of exf.LT/AP-g-p(DEAEMA)

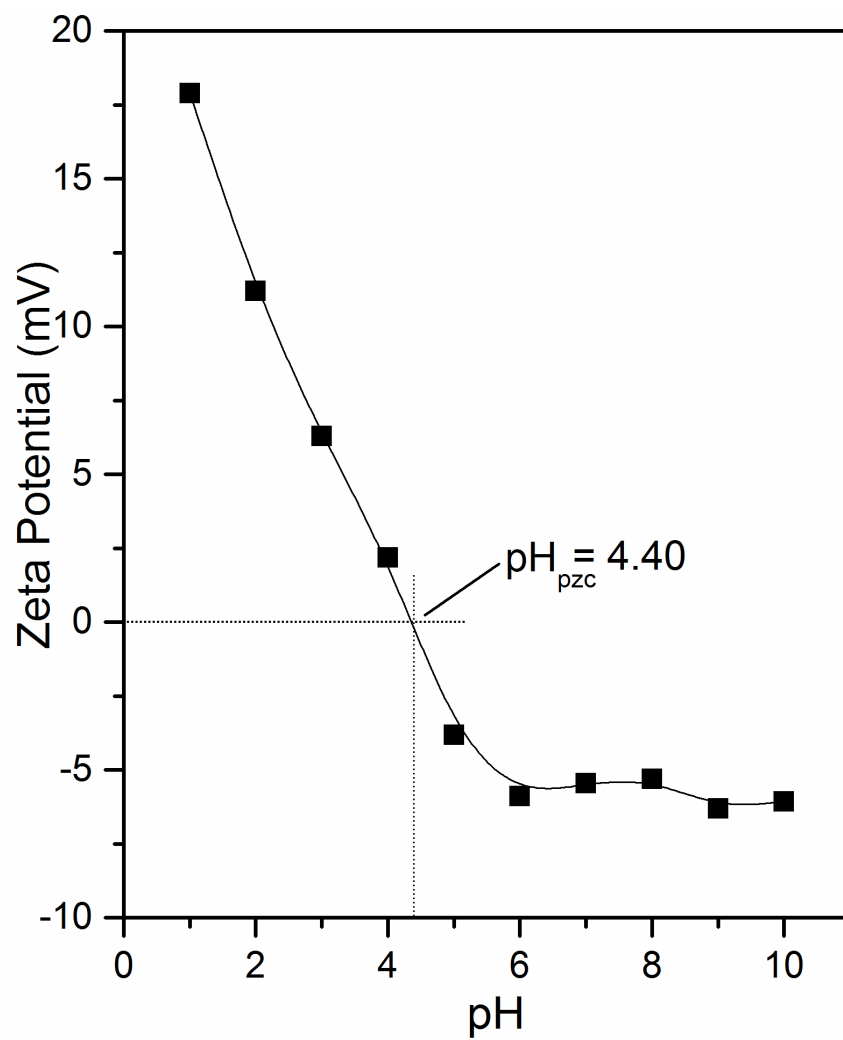


**Fig. S20.** pH dependency surface potentials of exf.LT/AP-g-p(DEAEMA) composite

**Table S3.** Hydrodynamic radius of AP-g-p(DEAEMA) and exf.LT/AP-g-p(DEAEMA) at pH: 3 and pH: 9

Nanocomposite	pH	Hydrodynamic diameter (d) (nm)
<i>exf.LT/AP-g-p(DEAEMA)</i>	3	1699
<i>exf.LT/AP-g-p(DEAEMA)</i>	9	377

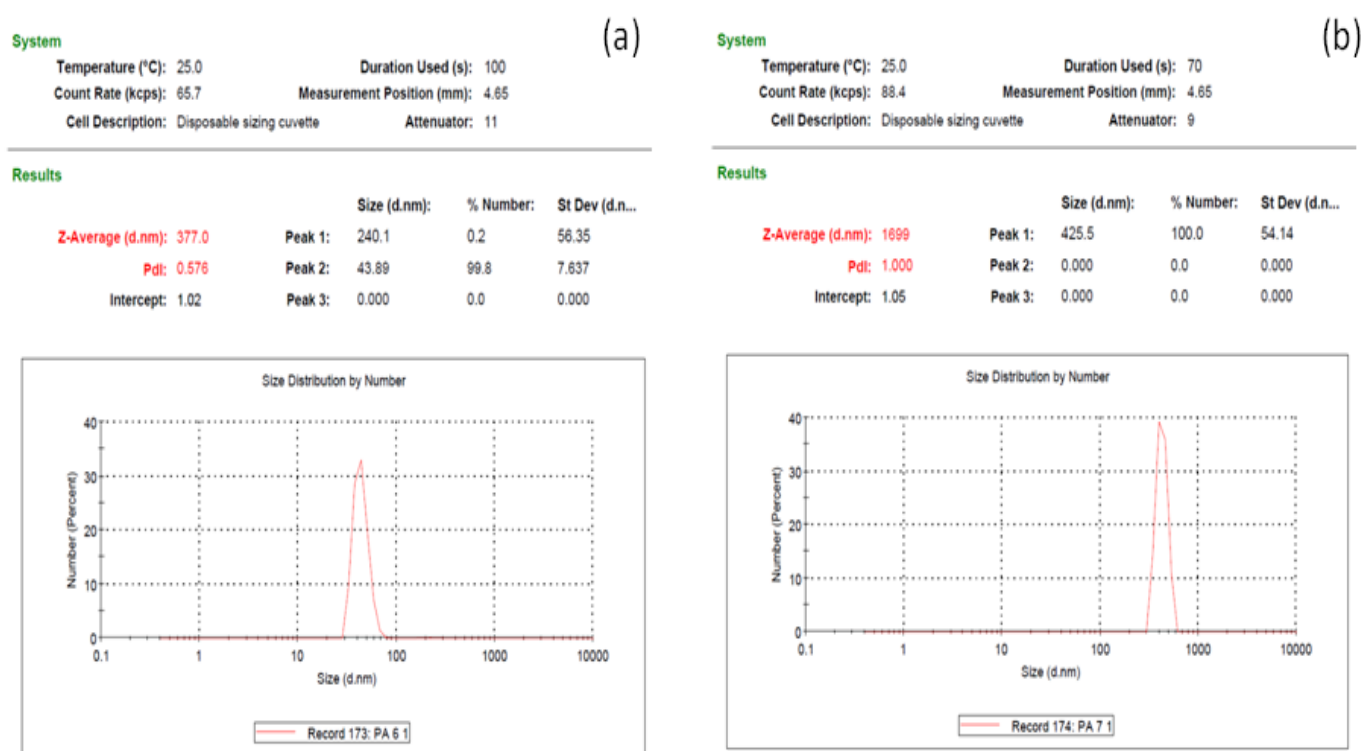


**Fig. S21.** DLS analysis result of exf.LT/AP-g-p(DEAEMA) at (a) pH-9 and (b) pH- 3

**FESEM analyses of dye loaded nanocomposite:**

FESEM analyses were performed to evaluate the morphological features of dye loaded adsorbents (Fig. S22). The accumulation of respective dyes on the surface of exf.LT/AP-g-

p(DEAEMA) was confirmed by the formation of shiny smooth surfaces. The layered particle like morphology of exf.LT/AP-g-p(DEAEMA) was changed to form smooth and shiny morphology, which is mainly because of the major accumulation of dyes on the composite surface. This characteristic feature suggests that physical interaction is mainly responsible between adsorbate and adsorbent. Also an efficient regeneration nature of adsorbent implies that electrostatic interaction between the active sites of adsorbent and adsorbate are accountable for an efficient adsorption process. Present study reveals that the rate of adsorption of MO, RB, MB, MG was initially found to be rapid and afterwards slowed down. The rapid and efficient removal was observed mainly because of the surface adsorption.

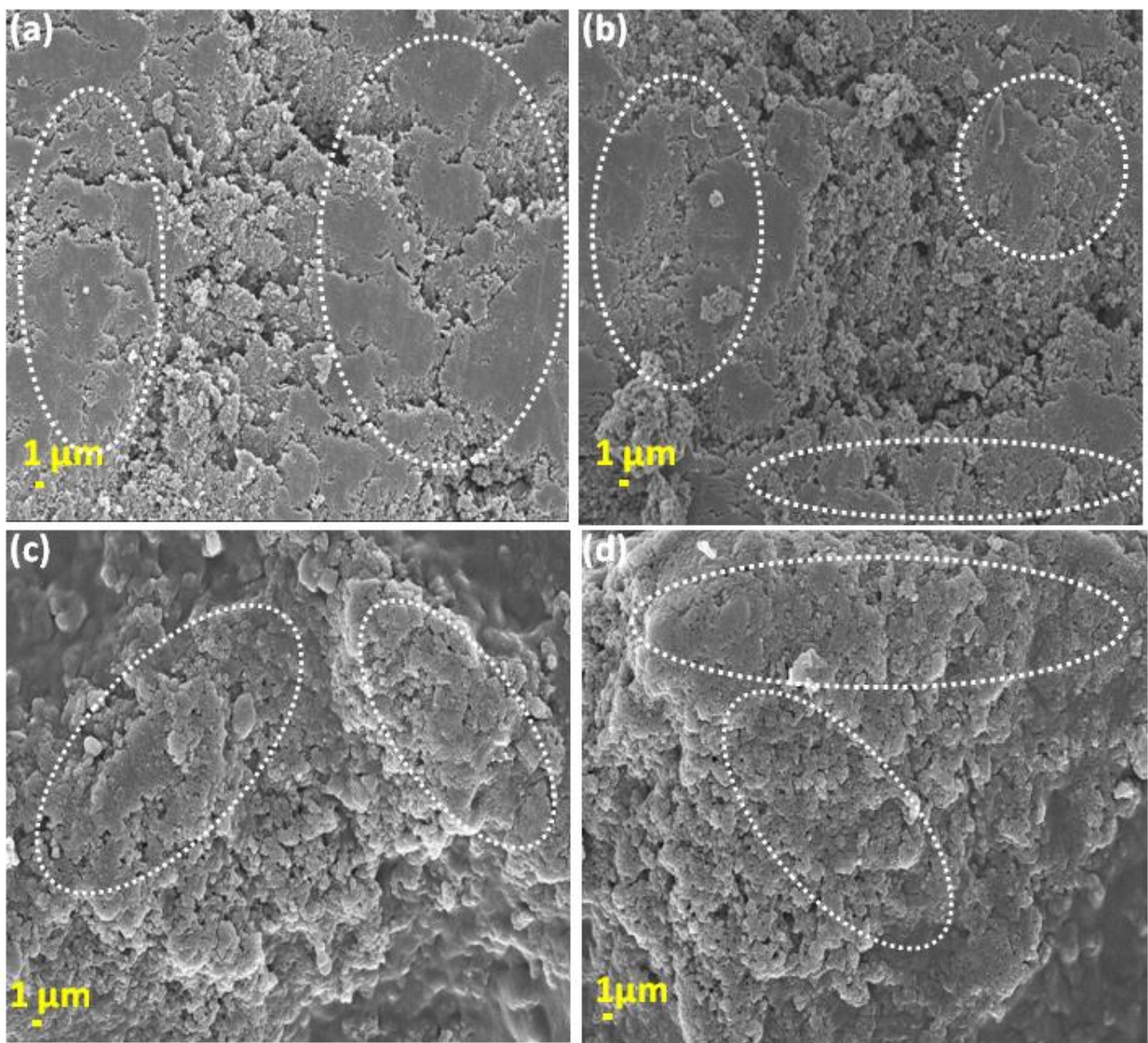


**Fig. S22.** FESEM images of (a) MO, (c) RB, (d) MB, and (e) MG adsorbed exf.LT/AP-g-p(DEAEMA)

## Adsorption Kinetics:

Pseudo second order and intraparticle diffusion models were used to examine the adsorption kinetics for RB, MO, MB, MG uptake on exfoliated nanocomposite. Pseudo second order kinetic model explains the interactive behavior of dyes and composite material.<sup>11</sup> Here, kinetic data of examined dyes were best fitted onto pseudo second order kinetic model. The equation is,

$$\frac{t}{q_t} = \frac{1}{k_2 q_e^2} + \frac{t}{q_e} \text{ ----- eq(1)}$$

Where,  $k_2$  ( $\text{g mg}^{-1} \text{min}^{-1}$ ) represents a corresponding rate constant. The parameters were evaluated by the plots of  $t/q_t$  vs.  $t$  (Fig. S23). The kinetics parameters are given at Table S3. The well fitted straight line at different RB, MO, MB, MG dye concentrations emphasized the agreement of experimental data. For each dye, correlation coefficients were found to be greater than  $>0.999$ . The kinetics data obtained from present study reveals that at equilibrium, solute would accumulate in adsorbent surface i.e. surface adsorption predominates. The adsorption capacity of MB/MG was increased with increases in initial dye concentration (Table S4). In another section amount of dye adsorbed ( $q_t$ ) vs. square root of time ( $t^{1/2}$ ) was plotted (Fig. S23), which exhibits an intersection of two straight lines.<sup>7,12</sup> Thus, it can be concluded that more than one step may control the total adsorption process. This model is intraparticle diffusion and the linear form is,

$$q_t = k_4 t^{1/2} + c \text{ ----- eq(2)}$$

Where  $k_4$  indicates intraparticle diffusion rate constant. First linear segment for MO and RB was appeared at initial 25 and 20 min. For MB and MG, the linear segment was found at initial 12 and 15 min. The first linear segment suggests that boundary layer diffusion predominates due to surface adsorption. Second segment follows intraparticle diffusion on porous surface of the

composite. Additionally, an intercept value (Table S4) indicates the thickness of the boundary layer. Thus it is apparent that surface adsorption along with intra particle diffusion probably play crucial role towards total adsorption process.

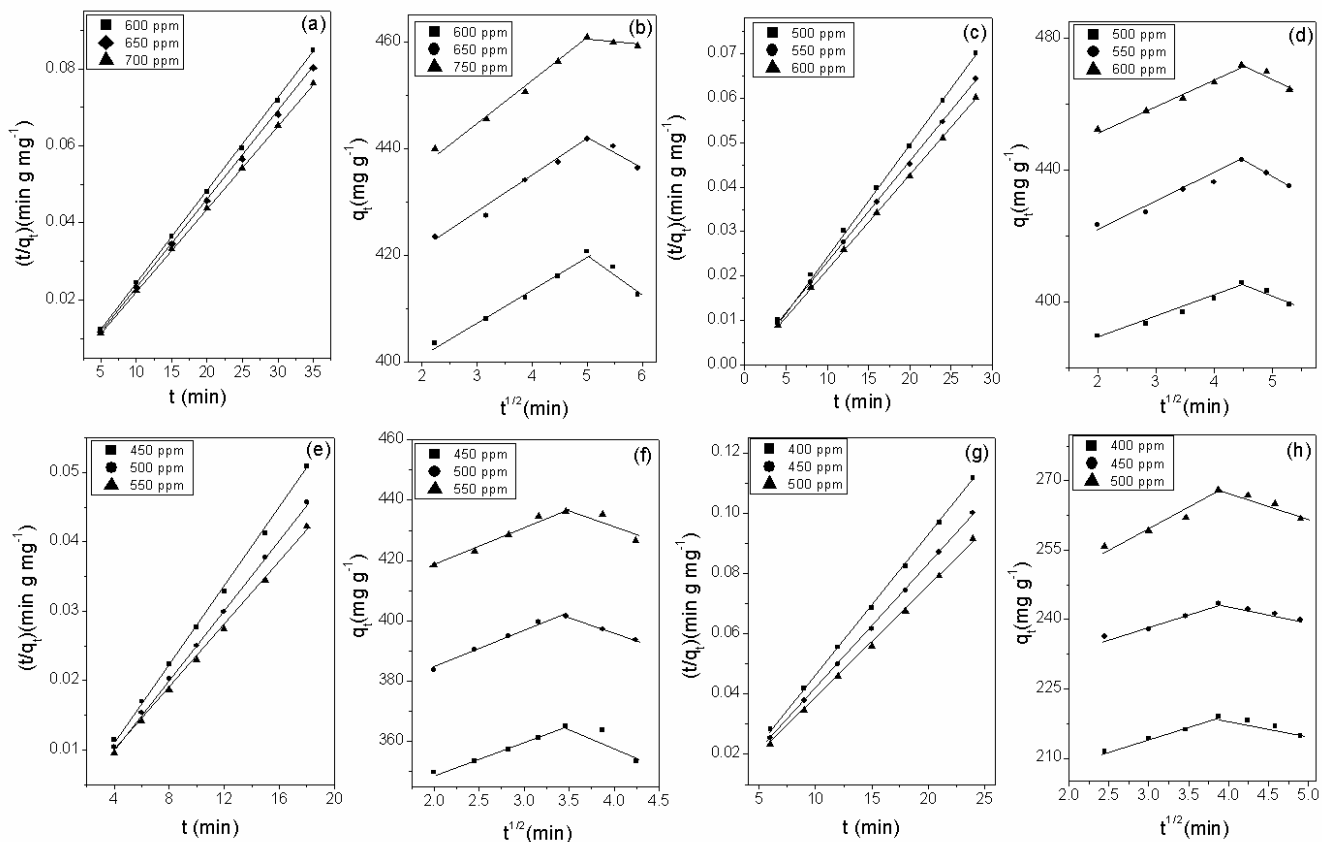


**Fig. S23.** Modeling of the adsorption kinetics of MO, RB, MB and MG using (a), (c), (e), (g) as pseudo-second-order and (b), (d), (f), (h) as intra-particle diffusion onto exf.LT/AP-g-p(DEAEMA)

**Table S4.** Kinetics parameters for adsorption of MO, RB, MB, MG dyes using exf.LT/AP-g-p(DEAEMA) adsorbent

Conc. (ppm)	Dye	Pseudo second order			Intraparticle diffusion		
		R <sup>2</sup>	K <sub>1</sub> (g.mg <sup>-1</sup> min <sup>-1</sup> )	q <sub>e</sub> (mg.g <sup>-1</sup> )	R <sup>2</sup>	K <sub>1</sub> (mg.g <sup>-1</sup> min <sup>0.5</sup> )	C (mg.g <sup>-1</sup> )
600		0.99962	15.94 × 10 <sup>-3</sup>	418.41	0.98304	6.10	389.19
650	MO	0.99952	9.66 × 10 <sup>-3</sup>	442.47	0.98151	6.77	407.44
700		0.99941	5.83 × 10 <sup>-3</sup>	465.11	0.98105	7.58	422.22
500		0.99975	1.60 × 10 <sup>-2</sup>	404.85	0.97028	6.41	375.95
550	RB	0.99969	1.41 × 10 <sup>-2</sup>	440.52	0.96803	7.62	406.57
600		0.99965	1.33 × 10 <sup>-2</sup>	469.48	0.98012	7.69	436.44
450		0.99985	1.02 × 10 <sup>-1</sup>	359.71	0.99249	10.52	328.05
500	MB	0.99944	0.37 × 10 <sup>-1</sup>	398.40	0.98320	12.42	359.50
550		0.99913	0.31 × 10 <sup>-1</sup>	432.90	0.97969	12.95	392.27
400		0.99969	6.80 × 10 <sup>-2</sup>	217.39	0.98443	5.19	198.63
450	MG	0.99947	4.73 × 10 <sup>-2</sup>	242.13	0.9470	5.31	223.55
500		0.99911	2.34 × 10 <sup>-2</sup>	266.66	0.92356	8.20	235.01

## Adsorption Isotherm:

Adsorption isotherm is essential for designing the operating system and correlates the equilibrium adsorption of dye molecules towards solid and liquid phase. For Isotherm study, batch experiments were performed with optimized conditions. The optimum temperature is 313K for MO and 318K for RB, respectively. For both MG and MB, the optimum temperature was 303K. A set of RB, MO, MB, MG solutions were prepared for examined the maximum adsorption capacity of respective dyes. For investigating adsorption isotherm, Langmuir<sup>13</sup> (eq. 3) and Freundlich<sup>14</sup> (eq. 4) models were used under study. The Langmuir<sup>13</sup> equation is,

$$\frac{c_e}{q_e} = \frac{1}{q_m b} + \frac{c_e}{q_m} \text{ ----- eq (3)}$$

Where,  $q_e$  (mg. g<sup>-1</sup>) and  $C_e$  (mg. L<sup>-1</sup>) denote amount of dye adsorbed at equilibrium and dye concentration, respectively.  $b$  (L. mg<sup>-1</sup>) is Langmuir constant, which was related to the affinity of binding sites.<sup>15</sup>  $q_m$  (mg. g<sup>-1</sup>) represents the theoretical monolayer adsorption capacity. Additionally, separation or equilibrium parameter ( $R_L$ ) was introduced to find out whether the isotherm is unfavorable ( $R_L > 1$ ), linear ( $R_L = 1$ ), irreversible ( $R_L = 0$ ) or favorable ( $0 < R_L < 1$ ).<sup>16</sup>

$$R_L = \frac{1}{1 + b \cdot C_0} \text{ ----- eq. (4)}$$

Where,  $b$  denotes as a Langmuir constant (L. mg<sup>-1</sup>) and  $C_0$  is the initial dye concentration (mg. L<sup>-1</sup>).

The linear form of Freundlich<sup>14</sup> equation is,

$$\ln q_e = \ln K_F + \frac{1}{n_F} \ln C_e \text{ ----- eq(5)}$$

$K_F$  (mg. g<sup>-1</sup>) and  $n_F$  denote Freundlich constants related to the adsorption capacity and adsorption strength, respectively. In Freundlich isotherm the value of  $n$  ( $0 < n_F < 10$ ) demonstrates whether the adsorption is favorable or not.

Fig.S24 reveals that Langmuir isotherm model shows a better fit with the experimental data in comparison with Freundlich isotherm model. Higher correlation co-efficient ( $R^2$ ) suggests that monolayer adsorption is predominate (Table S5). Also the values of  $R_L$  were found to be less than 1 (Table S6) and the value of  $n_F$  are found to be in between 1-10, suggesting the feasibility of the adsorption process. The Freundlich constant increased with rise in temperature, indicating the process is endothermic. With increase in temperature, the Langmuir constant “b” increased. This is mainly because of the stronger attraction between the active sites of the adsorbent and adsorbate. It also suggests that higher affinity between adsorbent and adsorbate molecules predominates at higher temperature in comparison with lower temperature.

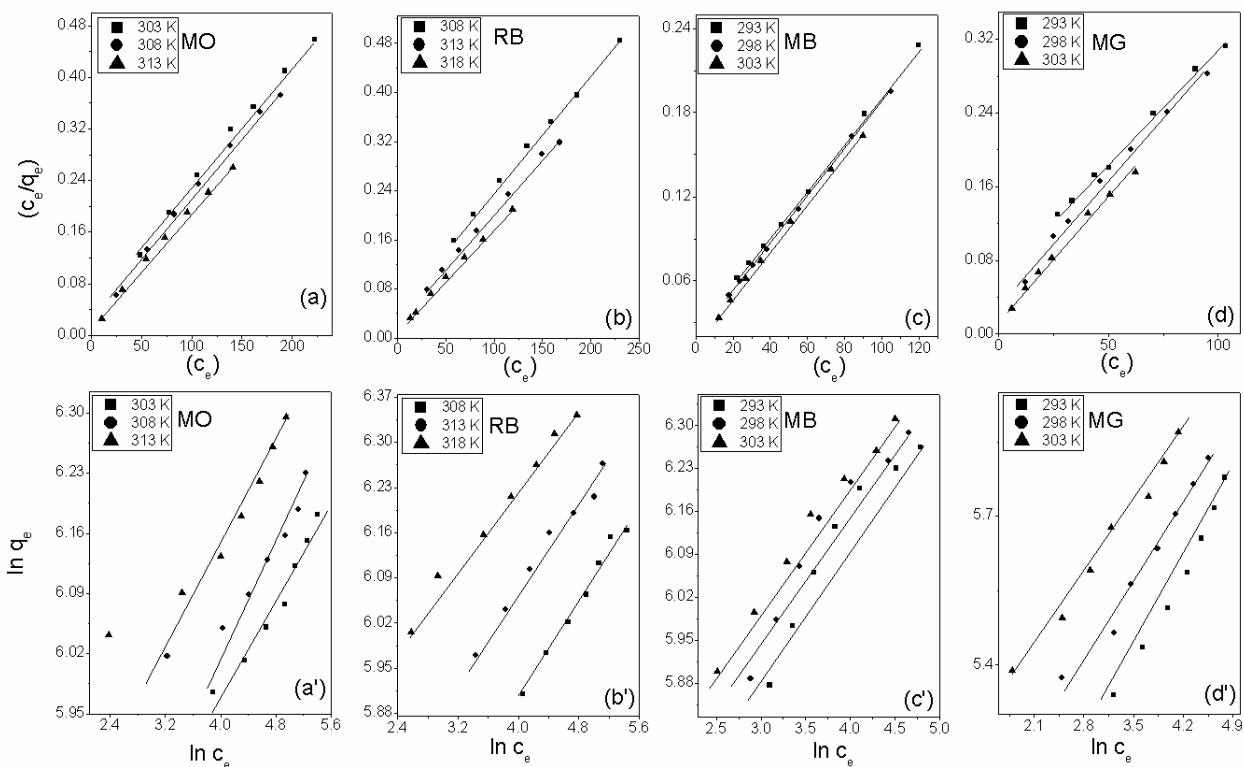


**Fig. S24.** Adsorption isotherm models fitted to experimental data for the adsorption of MO, RB, MB and MG at various temperatures using (a), (b), (c), (d) as Langmuir model and (a'), (b'), (c'), (d') as Freundlich isotherm model

**Table S5.** Parameters for Langmuir and Freundlich isotherm for various dye adsorptions.

Dye	Temp. (K)	Langmuir model			Freundlich model		
		$Q_{\max}$ ( $\text{mg}\cdot\text{g}^{-1}$ )	$b$ ( $\text{L}\cdot\text{mg}^{-1}$ )	$R^2$	$K_f$ ( $\text{mg}\cdot\text{g}^{-1}$ )	$n_f$	$R^2$
MO	303K	518.13	0.0479	0.9940	225.87	5.424	0.9492
	308K	526.31	0.0793	0.9945	286.86	9.764	0.8940
	313K	558.65	0.1216	0.9952	323.19	9.923	0.8907
RB	308K	534.75	0.0344	0.9969	167.84	5.159	0.9852
	313K	561.79	0.0642	0.9973	223.05	6.027	0.9784
	318K	598.80	0.1255	0.9980	279.82	6.693	0.9780
MB	293K	584.79	0.0752	0.9990	186.97	4.457	0.9322
	298K	591.71	0.0891	0.9993	201.92	4.625	0.9292
	303K	598.80	0.1088	0.9995	222.32	4.917	0.9438
MG	293K	377.35	0.0398	0.9961	84.18	3.627	0.9852
	298K	373.13	0.0771	0.9976	120.18	4.484	0.9765
	303K	380.22	0.1504	0.9979	149.48	4.894	0.9752

**Table S6.** Different  $R_L$  values at optimized condition.

Dye	Optimized Temp.	Optimized Conc. (ppm)	$R_L$
MO	313 K	600	0.0135
RB	318 K	500	0.0156
MB	303K	450	0.0200
MG	303K	400	0.0163

## Thermodynamics study:

Vant Hoff's equations (eq. 6-7) are used to establish the effect of temperature for adsorption of both classes of dyes.

$$\ln b = \frac{\Delta S^{\circ}}{R} - \frac{\Delta H^{\circ}}{RT} \text{ ----- eq. (6)}$$

$$\Delta G^{\circ} = \Delta H^{\circ} - T\Delta S^{\circ} \text{ ----- eq. (7)}$$

$b$ ,  $\Delta G^{\circ}$ ,  $\Delta S^{\circ}$ ,  $\Delta H^{\circ}$  are known as a Langmuir constant, change in standard Gibbs free energy (J. mol<sup>-1</sup>), change in entropy (J. mol<sup>-1</sup>. K<sup>-1</sup>) and change in enthalpy (J. mol<sup>-1</sup>), respectively.  $R$  and  $T$  denote as universal gas constant (8.314 J. mol<sup>-1</sup>. K<sup>-1</sup>) and temperature (K), respectively. The values of  $\Delta S^{\circ}$  and  $\Delta H^{\circ}$  were evaluated from the plot between  $\ln b$  vs.  $1/T$  (Fig. S25). Negative values of  $\Delta G^{\circ}$  for both classes of dyes indicate the feasibility and spontaneous nature of adsorption process. It has also been observed (Table S7) that with increase in experimental temperature,  $\Delta G^{\circ}$  values decreased. The negative values of  $\Delta G^{\circ}$  emphasized that higher degree of spontaneity at higher temperature. Endothermic nature of dye adsorption process was confirmed by positive values of enthalpy change.<sup>17</sup> Positive entropy change reveals that with increase in temperature, randomness was increased. This phenomenon signifies the efficient interaction between active sites of adsorbent and dye molecules.

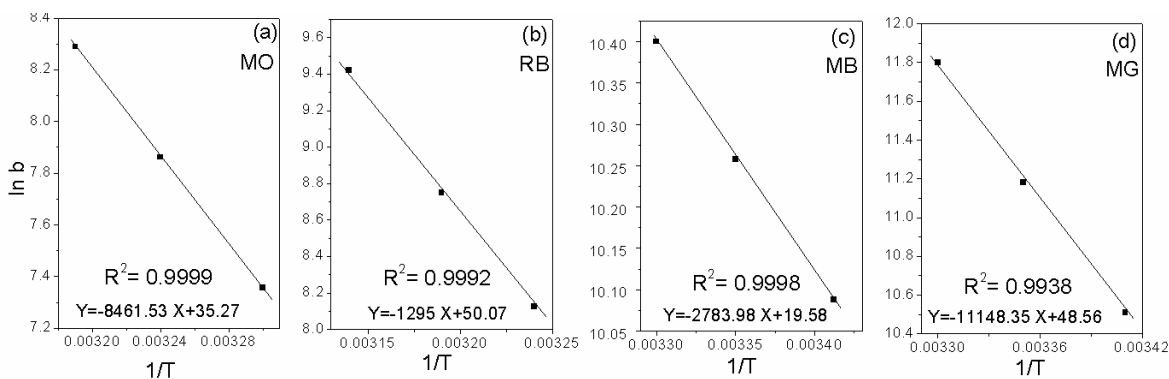


**Fig. S25.**  $\ln b$  vs.  $1/T$  plot for the adsorption of (a) MO (b) RB (c) MB (d) MG on exf.LT/AP-g-p(DEAEMA)

**Table S7.** Thermodynamic parameters for uptake of various dyes using exf.LT/AP-g-p(DEAEMA)adsorbent

Dye	Temp. (K)	$\Delta G^\circ$ (KJ mol <sup>-1</sup> )	$\Delta H^\circ$ (KJ mol <sup>-1</sup> )	$\Delta S^\circ$ (KJ mol <sup>-1</sup> K <sup>-1</sup> )
MO	303K	-18.520		
	308K	-19.992	70.349	0.2933
	313K	-21.458		
RB	308K	-20.557		
	313K	-22.635	107.666	0.4163
	318K	-24.717		
MB	293K	-24.554		
	298K	-25.368	23.146	0.1628
	303K	-26.182		
MG	293K	-25.392		
	298K	-27.615	92.687	0.4037
	303K	-29.634		

### Regeneration study:

Desorption is a well-known characteristic property of an efficient adsorbent. Desorption study was performed with three different media of pH 2.5, 7 and 10.5. For RB/MO dyes, maximum desorption was observed at pH10.5 and minimum % desorption was obtained at pH2.5. For MB/MG dyes, maximum and minimum % desorption were observed at pH 2.5 and pH10.5, respectively (Fig. S26). These characteristic results are completely opposite to that of adsorption

process. Afterwards, the desorbed dye concentration was measured by UV-VIS spectrophotometer (Table S8).

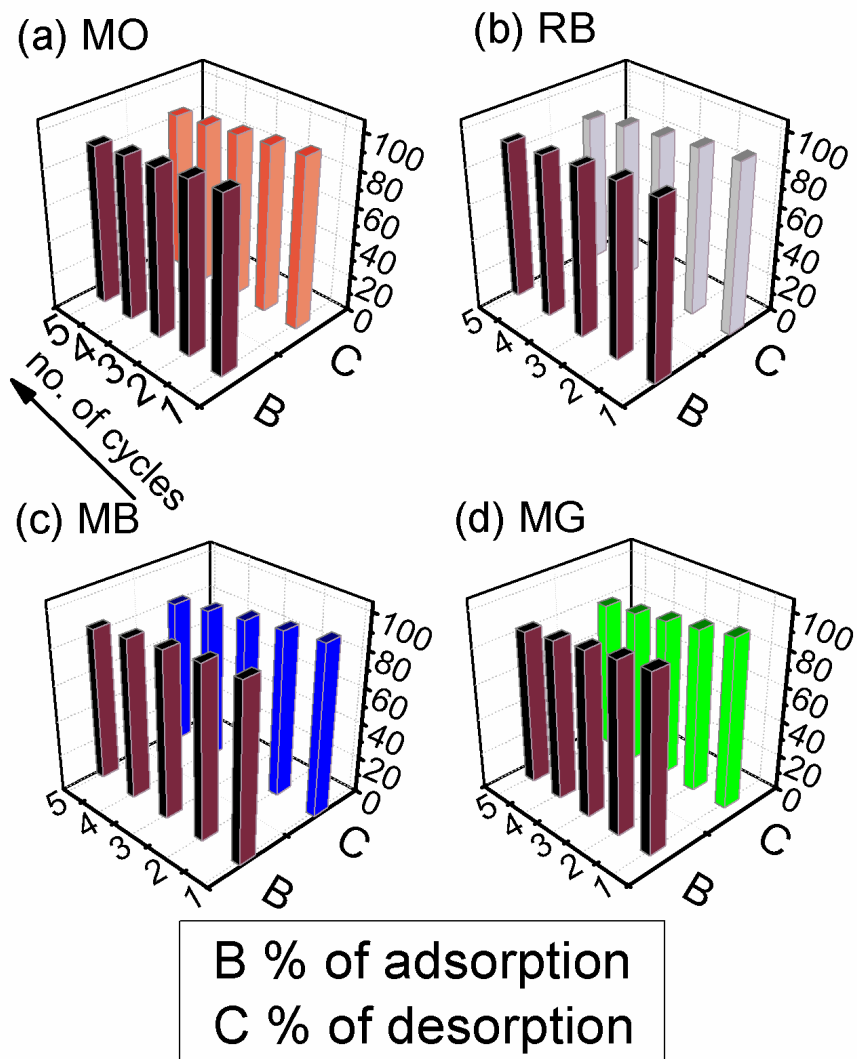


**Fig. S26.** Consequent adsorption-desorption cycles for (a) MO (b) RB (c) MB (d) MG using exf. LT/AP-g-p(DEAEMA)

**Table S8.** Adsorption and desorption characteristics of dyes on *exf.LT/AP-g-p*(DEAEMA)

Dye	Cycle	% Adsorption	% Desorption
MO	1	98.20	96.01
	2	96.42	94.12
	3	94.01	92.18
	4	92.12	90.01
	5	89.52	88.18
RB	1	97.35	95.35
	2	95.78	93.18
	3	93.29	90.27
	4	90.12	87.39
	5	87.89	83.08
MB	1	97.26	95.12
	2	95.48	92.31
	3	92.54	89.17
	4	89.14	85.43
	5	85.07	81.18
MG	1	98.50	95.18
	2	95.92	91.42
	3	92.48	88.39
	4	89.28	85.12
	5	86.17	82.18

For regeneration study via degradation, the dye loaded material was decolorized under exposure of UV light (Fig. S27). Five consecutive cycles were performed for the degradation study. It was found that after 5<sup>th</sup> cycles, no appreciable loss occurs in degradation efficiency (Table S9).

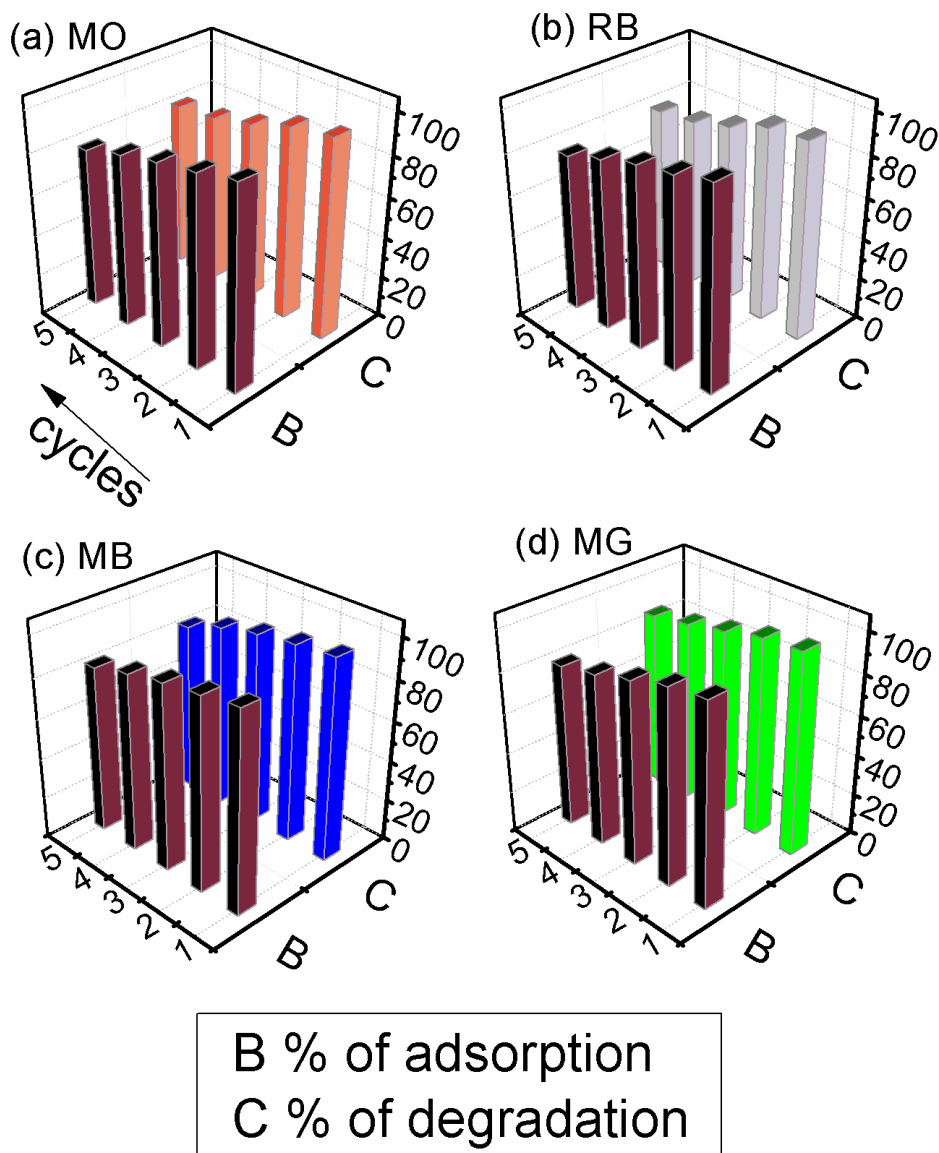


**Fig.S27.** Consequent adsorption-degradation cycles for (a) MO (b) RB (c) MB (d) MG using exf.LT/AP-g-p(DEAEMA)

**Table S9.** Degradation cycles for (a) MO (b) RB (c) MB (d) MG using exf.LT/AP-g-p(DEAEMA)

Dye	Cycle	% Degradation
MO	1	95.41
	2	92.64
	3	87.12
	4	82.36
	5	75.23
RB	1	94.12
	2	91.01
	3	86.28
	4	80.36
	5	74.19
MB	1	94.18
	2	91.24
	3	88.75
	4	84.36
	5	80.41
MG	1	94.03
	2	90.18
	3	87.03
	4	83.25
	5	79.15

After 120 min, the solutions of MO and after 60 min, the solution of MB were totally decolorized (Fig. S28). TiO<sub>2</sub> itself used as a photocatalytic degradation agent under UV irradiation. Previously biopolymer based TiO<sub>2</sub> nano particles were used for degradation of different classes of dyes.<sup>18</sup> Principally, single sheet of titanate can involve in photoexcitation by UV light irradiation. These photo induced electrons can generate positive holes. Then the holes react with electron donor or water molecules to produce the free radicals.<sup>19</sup> These free radicals are capable of degrading organic dye molecules. Positive holes were generated when electrons were jump to the conduction band. After desorption, complete removal of dye was occurred via degradation. The weight loss of adsorbent during the desorption process is the main reason for lowering the % of adsorption in each cycle. Hence to determine the regeneration efficacy, five desorption-degradation cycles were performed.

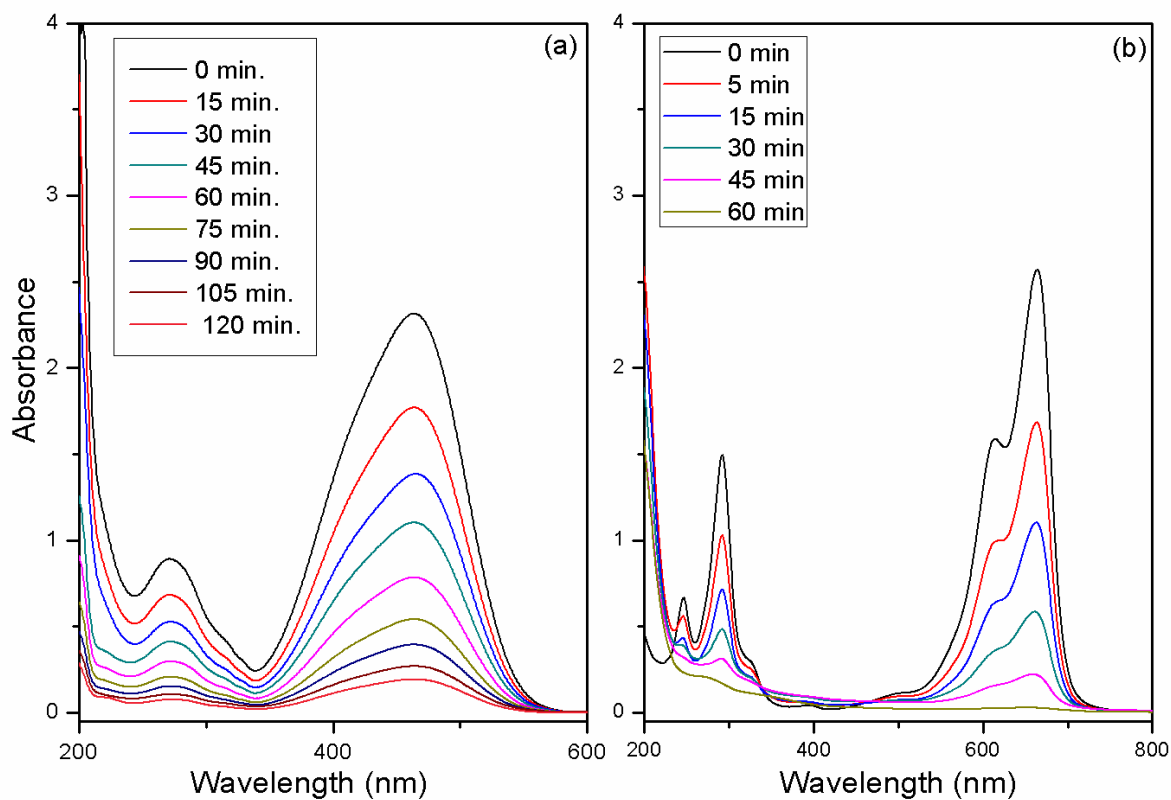


**Fig. S28.**Photocatalytic degradation of (a) MO and (b) MB using exf.LT/AP-g-p(DEAEMA)

**Table S10.** Comparison of adsorption capacity of various reported adsorbents

Adsorbent material	Selective Adsorption <sup>a</sup> (mg g <sup>-1</sup> )		Deg. <sup>b</sup>	Ref.
	Cationic dye (MB)	Anionic dye (MO)		
<b>exf.LT/AP-g-p-DEAEMA</b>	<b>598.80</b>	<b>558.65</b>	<b>Y</b>	<b>Present Work</b>
ErCu–POM (Er-3)	391.3	No Ads.	N	20
Polyphosphazene	142.46	No Ads.	N	21
phthalic acid hydrogel	~800 <sup>**</sup>	No Ads.	N	22
DBS hydrogel	770	No Ads.	N	23
Resoecin polymer	3.6	No Ads.	N	24
Layered titanate	184	No Ads.	Y	25
PW11V@MIL-101	371	No Ads.	N	26
Mg-silicate- RGO	433	No Ads.	N	27
TiO <sub>2</sub> -CoFe <sub>2</sub> O <sub>4</sub> -P.aniline	No Ads.	168.57	N	28
Activated CNT	399	149	N	29
GO–MWCNT	298	294	N	30

<sup>a</sup>Selective Adsorption, <sup>b</sup>Photocatalytic degradation <sup>\*\*</sup> needs hazardous organic solvent for desorption.

## References:

- [1] D. Roy, M. Semsarilar, J. T. Guthrie and S. Perrier. *Chem. Soc. Rev.*, 2009,**38**, 2046-2064.
- [2] N. Sutradhar, A. Sinhamahapatra, S. K. Pahari, H. C. Bajaj and A. B. Panda. *Chem. Commun.*,2011, **47**, 7731-7733.
- [3] Y. Wang, J. Chen, L. Lu, and Z. Lin. *ACS Appl. Mater. Interface.*, 2013, **5**, 7698-7703.
- [4] X. He, K. B. Male, P. N. Nesterenko, D. Brabazon, B. Paull, and J. H.T. Luong. *ACS Appl. Mater. Interfac.*, 2013, **5**, 8796-8804
- [5] J. Zhao, T. Wu, K. Wu, K. Wa, H. Hidaka and N. Serpone. *Environ. Sci. Technol.*, 1998, **32**, 2394-2400.
- [6] A. K. Sarkar, N. R. Mandre, A. B. Panda and S. Pal. *Carbohydr. Polym.*, 2013, **95**, 753-759.
- [7] A. K. Sarkar, A. Pal, S. Ghorai, N. R. Mandre and S. Pal. *Carbohydr. Polym.*, 2014, **111**, 108-115.
- [8] N. Sukpirom and M. M. Lerner. *Chem. Mater.*, 2001, **13**, 2179-2185.
- [9] X. Huang, D. Appelhans, P. Formanek, F. Simon and B. Voit. *ACS Nano.*, 2012, **6**, 9718-9726.
- [10] M. S. Bootharaju and T. Pradeep. *Langmuir*, 2013, **29**, 8125-8132.
- [11] Y. S. Ho, G. McKay, *Process Biochem.*, 1999, **34**, 451-465.
- [12] S. Ghorai, A. Sarkar, M. Raoufi, A. B. Panda, H. Schönherr and S. Pal. *ACS Appl. Mater. Interfac.*, 2014, **6**, 4766-4777.
- [13] I. Langmuir, The constitution and fundamental properties of solids and liquids. *Journal of American Chemical Society.*, 1916, **38**,2221-2295.

- [14] H.M.F. Freundlich, Uber die adsorption in Losungen, *Z. Phys. Chem.*, 1906, **57**, 385-470.
- [15] C. H. Wu. *J. Hazard. Mater.*, 2007, **144**, 93-100.
- [16] M.M. Ayad and A. A. E. Nasr. *J. Phys. Chem C.*, 2010, **114**, 14377-14383.
- [17] S. Chowdhury, R., Mishra, P. Saha, and P. Kushwaha. *Desalination*, 2011, **265**, 159-168.
- [18] D. Mahanta, U. Manna, G. Madras S. Patil. *ACS Appl. Mater. Interfac.*, 2011, **3**, 84-92.
- [19] K. V. Baiju, S. Shukla, K. S. Sandhya, J. James, K. G. K. Warriar. *J. Phys. Chem. C.*, 2007, **111**, 7612-7622
- [20] F. -Y. Yi, W. Zhu, S. Dang, J. -P. Li, D. Wu, Y.-h. Li, Z.-M. Sun. *Chem. Commun.*, 2015, **51**, 3336-3339.
- [21] W. Wei, R. Lu, H. Xie, Y. Zhang, X. Bai, L. Gu, R. Da, X. Liu, *J. Mater. Chem. A*, 2015, **3**, 4314-4322.
- [22] F. R.-Llansola, B. Escuder, J. F. Miravet, D. H.-Merino, I. W. Hamley, C. J. Cardin, W. Hayes. *Chem. Commun.*, 2010, **46**, 7960–7962
- [23] B. O. Okesola and D. K. Smith. *Chem. Commun.*, 2013, **49**, 11164–11166.
- [24] L. L. Lv, J. Yang, H-M. Zhang, Liu Y-Y. Ma. *J. F. Inorg. Chem.*, 2015, **54**, 1744-1755.
- [25] N. Sutradhar, A. Sinhamahapatra, S. K. Pahari, H. C. Bajaj, A. B. Panda. *Chem. Comm.*, 2011, **47**, 7731.
- [26] X. Yan, S. Yao, Y. G. Li, Z. M. Zhang, Y. Lu, W. L. Chen, E. B. Wang. *Chem. Eur. J.*, 2014, **20**, 6927–6933.
- [27] C. Gui, Q. Wang, S. Hao, J. Qu, P. Huang, C. Cao, W. Song, Z. Yu, *ACS Appl. Mater. Interfac.*, 2014, **6**, 14653–14659.
- [28] P. Xiong, L. Wang, X. Sun, B. Xu, X Wang. *Ind. Eng. Chem. Res.*, 2013, **52**, 10105–10113.

- [29] J. Ma, F. Yu, L. Zhou, L. Jin, M. Yang, J. Luan, Y. Tang, H. Fan, Z. Yuan, J. Chen.  
*ACS Appl. Mater. Interfac.*, 2012, **4**, 5749-5760.
- [30] C. Sarkar, C. Bora and S. K. Dolui, *Ind. Eng. Chem. Res.*, 2014, **53**, 16148–16155.